C.P. No. 397
(19,547)
A R C Technical Report

C.P. No. 397
(19,547)
A R C. Technical Report

MINISTRY OF SUPPLY

AERONAUTICAL RESEARCH COUNCIL

CURRENT PAPERS

Some Methods of Evaluating Imperfect Gas Effects in Aerodynamic Problems

by

G. A. Bird

LONDON HER MAJESTY'S STATIONERY OFFICE

1958

PRICE 4s. 6d NET

C.P. No. 397

U.D.C. No. 533.6.011 : 533.6.011.72

Technical Note No. Aero 2488

January, 1957

ROYAL AIRCRAFT ESTABLISHMENT

Some methods of evaluating imperfect gas effects in aerodynamic problems

by

G. A. Bird

SUMMARY

Simple numerical and graphical procedures are described for the calculation of the imperfect gas effects on the properties of steady and unsteady one-dimensional isentropic flows, the Prandtl-Meyer expansion round a corner and normal and oblique shock waves. The fundamental equations of each type of flow have been put into a form in which they may be solved using the published tables of the equilibrium properties of gases. Both thermal and caloric imperfections have been taken into account but relaxation time effects have been neglected.

Numerical examples are given for each type of flow although the main emphasis has been placed on the methods rather than on the results. These basic methods have been used to calculate the magnitude of the imperfect gas effects on a number of specific aerodynamic problems which have been considered in detail.

LIST OF CONTENTS

LIST OF ILLUSTRATIONS

1 Introduction

In the last few years, the high temperatures that have been encountered in aerodynamic problems have been such that it has become necessary to consider the effects produced by the difference in behaviour of a real gas compared with that of a 'perfect' gas.

A perfect gas is here defined as one which has constant specific heats (caloric perfection) and which obeys the equation of state $\frac{p}{\rho} = \frac{R}{m} T$ (thermal perfection). At low temperatures or high pressures, a real gas departs from the perfect gas equation of state as a result of molecular force and molecular size effects becoming apparent. At considerably higher temperatures, appreciable energy is imparted to additional degrees of freedom and then specific heats then cease to be constant. At still higher temperatures, the composition of the gas may change as a result of molecular dissociation and cause variation in the specific heats and in the molecular weight. Molecular ionisation does not commence to produce appreciable effects until even higher temperatures have been reached.

A large number of attempts have been made to modify the conventional gas dynamic equations so that they apply to real as well as perfect gases. Some aspects of the problem have been treated by the use of one of the more nearly exact equations of state such as van der Waal's in reference 1, Berthelot's in reference 2 and the Beattie-Bridgeman equation in reference 3, and allowance was made in several of these reports for changes in the specific heat ratio also. Some other methods have been suggested which allow for changes in the specific heat ratio only. However, this type of treatment does not take into account all types of imperfection and, in general, it is restricted to flows in which dissociation does not occur. The expressions which are obtained by these methods are invariably extremely involved and it is not easy to apply them to the specific problems which are encountered in practice.

A number of sets of tables have recently been issued which list the equilibrium thermal properties of gases (such as entropy, enthalpy, density etc.) as functions of temperature and pressure. For instance, reference 4 lists them for air up to temperatures of 5000°K and pressures of 100 atmospheres and, in reference 5, data is tabulated for a number of gases. Both these sets of tables are based on the now obsolete value of 7.373 e.v. per molecule for the dissociation energy of nitrogen, but reference 6 gives a preliminary form of revised tables based on the currently accepted value of 9.758 e.v. per molecule*. These tables take into account (as far as is possible) all types of imperfection.

In references 7, 8 and 9, the normal shock wave equations are solved for a variety of initial conditions, by iterative methods which make direct use of these tables. However, it is assumed in all these methods that the gas is thermally perfect, i.e. the perfect gas equation of state still applies. This assumption is valid for combinations of high temperatures and low pressures even if the gas is dissociating, but it is not justified at low temperatures or high pressures. In section 2.21 of this report, a simple graphical method is presented for the solution of the shock wave equations for any initial conditions; the

---

* Unfortunately these tables were not available to the author at the time of preparation of this report and the older sets of tables have necessarily been used in the examples.

method uses the tabulated real gas properties which take into account thermal as well as caloric imperfections. The method is extended to cover oblique shock waves also. (Section 2.22).

References 7 and 8 present methods of dealing with imperfect gas effects on the propagation of one-dimensional unsteady isentropic waves. These are based on the replacement of the usual form of the Riemann variables $q \pm \frac{2}{\gamma-1} a$ which is valid only for an ideal gas by the more fundamental form $q \pm \int \frac{a}{\rho} d\rho$ which is valued for real gases also. This integral is not easy to evaluate in the real gas case, and has been tabulated for a few cases only. The method presented in Section 2.13 of the Report makes direct use of the more fundamental equation $\frac{dq}{dp} = \pm \frac{1}{\rho a}$ and a simple numerical procedure is given for the complete solution of the problem for any initial conditions.

Reference 7 considers also steady isentropic expansions and presents a method which is again very complicated and which depends upon the gas being thermally perfect. In Section 2.11 a graphical method is suggested which is consistent with that outlined above for unsteady flow. Euler's equation of motion for steady one-dimensional flow may be put into the form $\frac{d(\frac{1}{2} q^2)}{dp} = - \frac{1}{\rho}$ and the real gas tables enable this to be integrated directly along any required isentrope. A simple extension of the method is given in section 2.12 to cover the Prandtl-Meyer expansion round a corner.

It is not necessary to bring enthalpy into the isentropic flow calculations as has been done in references 7 and 8. No iteration procedures are involved in any of the methods presented in this Report and they are all far more straightforward than those which have previously been proposed, even though they allow for thermal as well as caloric imperfections.

The magnitude of the imperfect gas effects is dependent on the initial temperature and pressure of the gas to such an extent that it is practically impossible to compile a comprehensive set of compressible airflow tables for a real gas. Emphasis has therefore been put, in this Report, on the development and presentation of simple numerical procedures by which the imperfect gas effects may be calculated in any specific example. A number of examples are given which illustrate the application of these procedures to typical problems.

It has been assumed in all these methods that relaxation time effects may be neglected. These relaxation time effects arise because excitation of the various degrees of freedom of the molecules, the adjustment of energy in them, dissociation, reassociation, ionisation and recombination all occur as a result of collisions between molecules and atoms. A number of collisions is required to produce equilibrium and this number varies greatly with the type of process and the gas in which it is taking place. Equilibrium is reached very quickly between the translational and rotational degrees of freedom but a considerable number of collisions are required to reach equilibrium if the vibrational modes are excited and the fluid moves a certain distance whilst it is being established. Experiments have indicated that this "relaxation distance" rarely exceeds a few centimetres and is usually very much less and that it decreases as the temperature and pressure increase. Very little is known about rates of dissociation, although equilibrium is probably reached far more slowly than in the case of the vibrational energy adjustment. Still less is known about rates of reassociation and these will have a very pronounced effect on the flow in the nozzle of a hypersonic impulse tunnel. The importance of these non-equilibrium effects will depend on the ratio of a typical dimension of the flow to these

"relaxation distences", and much work remains to be done before the magnitude of these effects can be estimated in practical cases.

2 Methods of Analysis of Basic Flows

2.1 Isentropic processes

The conventional gas dynamic equations for one-dimensional isentropic flows are obtained from the equations of motion by use of the perfect gas isentropic relation between pressure and density $\left(\frac{p}{\rho^\gamma} = \text{const.}\right)$. In the following sections, the basic equations will be put into a form in which they may be integrated directly using the tabulated thermal properties of real gases.

2.11 Steady one-dimensional isentropic flow

Consider the flow in a stream tube. The momentum equation is

$$\frac{\partial q}{\partial t} + q\frac{\partial q}{\partial x} = -\frac{1}{\rho}\frac{\partial p}{\partial x} \qquad (2.1)$$

For steady flow $\frac{\partial q}{\partial t} = 0$ and, as only one dimension is involved, the equation may be written:

$$q\,dq = -\frac{1}{\rho}\,dp$$

or

$$\frac{d(\frac{1}{2}q^2)}{dp} = -\frac{1}{\rho} \qquad (2.2)$$

(For a perfect gas, this may be integrated to give the conventional energy equation).

The tables list specific entropy of a real gas as a function of temperature and pressure. The isentrope for the real gas may therefore be constructed by looking up the value of entropy for the initial conditions and then finding the values of temperature and pressure in the required range for which the value of the entropy is constant. As an example, the isentrope for air expanded from 5000°K and 100 atm is plotted in Figure 1.1 and is compared with that given by the perfect gas relation $\frac{p}{\rho^\gamma} = \text{constant}$. Density and speed of sound are also listed[4,5,6] as functions of temperature and pressure and curves of ρ and a (see Figs.1.3 and 1.2) may be plotted against p for these isentropes.

The reciprocal of the density $\left(\text{which by equation 2.2 is equal to } -\frac{d(\frac{1}{2}q^2)}{dp}\right)$ is then plotted against p in Fig.1.4 and these curves are integrated graphically to give curves of $\frac{1}{2}q^2$ against p (Fig.1.5). In this example the gas was assumed to be expanded from rest, but the initial value of $\frac{1}{2}q^2$ in the integration may be adjusted for any initial velocity. Once the relation between $\frac{1}{2}q^2$ and p has been found, that between q and p follows (Fig.1.6) and this is used in conjunction with the curve of a against p (Fig.1.2) to find the relation between Mach number and pressure (Fig.1.7).

The accuracy of the numerical and graphical procedures may be checked if the curves appropriate to the perfect gas are plotted alongside those

of the real gas in each figure. The two sets of curves were operated upon in exactly the same manner and an indication of the accuracy of the calculations was given by comparing the calculated values of p against M for the perfect gas with those given by the relation $\frac{p}{p_o} = \left(1 + \frac{\gamma-1}{2} M^2\right)^{\frac{-\gamma}{\gamma-1}}$.

The continuity equation gives

$$\frac{A}{A^*} = \frac{\rho^* q^*}{\rho q} \tag{2.3}$$

The pressure at which $M = 1$ is found from Fig.1.7 and ρ^* and q^* are then found from Figs.1.3 and 1.6 respectively. The area ratio $\frac{A}{A^*}$ may then be found as a function of Mach number and the results for the perfect gas again provided a check on the accuracy of the calculations.

In the example shown in Fig.1, there is considerable dissociation of the gas under stagnation conditions and the very large departures from perfect gas behaviour are a result of the subsequent reassociation. The energy which is released in the reassociation process causes the temperature, at a given pressure, to be much higher than in the case of a perfect gas expanded to the same pressure. The speed of sound is therefore much higher and the density is lower. The reciprocal of the density is higher and so the velocity produced by a given pressure drop is higher for the real gas. However, the effect on speed of sound is greater than that on velocity and the Mach number for a given pressure drop is less for the real gas than for the perfect gas. There is also a very pronounced real gas effect on area ratio, the real gas requiring a far greater area ratio to reach a given Mach number.

Figure 2 shows the corresponding results when the gas is initially at a temperature such that no dissociation or reassociation effects are encountered. There are differences of several percent between real and perfect gas cases in the pressure versus temperature, speed of sound, density and velocity curves but these are in directions such that they tend to cancel out when the Mach number versus pressure and area ratio curves are calculated from them.

2.12 Prandtl-Meyer expansion round corner

The equations of momentum for the steady flow of an inviscid compressible fluid may be written in polar coordinates as,

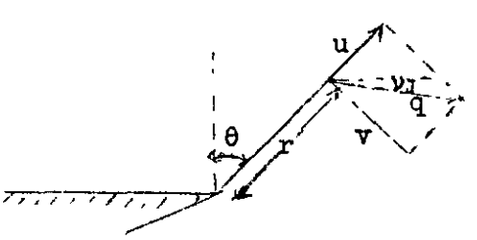

$$\frac{v}{r}\frac{\partial u}{\partial \theta} + u\frac{\partial u}{\partial r} - \frac{v^2}{r} = -\frac{1}{\rho}\frac{\partial p}{\partial r} \tag{2.4}$$

and

$$\frac{v}{r}\frac{\partial v}{\partial \theta} + u\frac{\partial v}{\partial r} + \frac{uv}{r} = -\frac{1}{\rho r}\frac{\partial p}{\partial \theta} \tag{2.5}$$

The equation of continuity is:

$$\frac{\partial}{\partial r}(\rho u r) + \frac{\partial}{\partial \theta}(\rho v) = 0 \tag{2.6}$$

In the case of supersonic flow, it may be assumed that p, ρ, u and v are functions of θ only and the equations then reduce to,

$$\frac{v}{r}\frac{\partial u}{\partial \theta} - \frac{v^2}{r} = 0$$

or

$$v = \frac{\partial u}{\partial \theta} \tag{2.7}$$

$$v\left(\frac{\partial v}{\partial \theta} + u\right) = -\frac{1}{\rho}\frac{\partial p}{\partial \theta} \tag{2.8}$$

and

$$\rho u + \rho \frac{\partial v}{\partial \theta} + v \frac{d\rho}{d\theta} = 0 \tag{2.9}$$

From (2.9),

$$\rho\left(u + \frac{\partial v}{\partial \theta}\right) = -v\frac{\partial \rho}{\partial \theta} = -\frac{v}{a^2}\frac{\partial p}{\partial \theta} \tag{2.10}$$

But from (2.8),

$$\rho\left(u + \frac{\partial v}{\partial \theta}\right) = -\frac{1}{v}\frac{\partial p}{\partial \theta} \tag{2.11}$$

Comparing (2.10) with (2.11),

$$v = a \tag{2.12}$$

Hence

$$u = \sqrt{q^2 - v^2} = \sqrt{q^2 - a^2} \tag{2.13}$$

and from (2.7) and (2.12),

$$\frac{d\theta}{du} = \frac{1}{a} \tag{2.14}$$

Equation (2.2) applies along a stream tube and the methods of section 2.11 are used to construct curves of a against p, q against p and M against p. Corresponding values of u and $\frac{1}{a}$ may then be found for any value of Mach number and these are plotted against one another as shown in Figure 3.1. As $\frac{1}{a} = \frac{d\theta}{du}$ (equation 2.14), these curves may be integrated graphically to give curves of θ against u (Fig.3.2) and the curves of θ against M (Fig.3.3) follow.

The flow deflection angle is given by,

$$\nu = \theta - \tan^{-1}\frac{u}{v}$$

$$= \theta - \tan^{-1}\sqrt{M^2 - 1} \tag{2.15}$$

The curves of ν against M are then plotted as shown in Fig.3.4 and the accuracy of the calculations may be checked by comparing the perfect gas values with those given by the conventional gas dynamics equation,

$$\nu = \sqrt{\frac{\gamma+1}{\gamma-1}}\tan^{-1}\sqrt{\frac{\gamma-1}{\gamma+1}}\sqrt{M^2-1} - \tan^{-1}\sqrt{M^2-1}$$

The example shown in Figs.3.1 to 3.4 is for air expanded from a temperature of 5000°K and a pressure of 100 atmospheres, and reassociation again produces large imperfect gas effects. Figure 3.5 shows the corresponding effect on Prandtl-Meyer angle when the stagnation temperature is much lower and, in the absence of initial dissociation, the departures from the perfect gas values are of the order of one or two percent only.

2.13 Propagation of one-dimensional isentropic wave

The continuity equation may be written,

$$\frac{\partial\rho}{\partial t} + \rho\frac{\partial q}{\partial x} + q\frac{\partial\rho}{\partial x} = 0, \qquad (2.16)$$

and the momentum equation may again be written,

$$\frac{\partial q}{\partial t} + q\frac{\partial q}{\partial x} + \frac{1}{\rho}\frac{\partial p}{\partial x} = 0 \qquad (2.1)$$

Treating p as a function of ρ and S,

$$\partial p = \left(\frac{\partial p}{\partial S}\right)_\rho \partial S + \left(\frac{\partial p}{\partial \rho}\right)_S \partial\rho$$

i.e. $$\left(\frac{\partial p}{\partial S}\right)_\rho = \frac{\partial p}{\partial S} - a^2\frac{\partial\rho}{\partial S} \qquad (2.17)$$

and, as the flow is isentropic,

$$\frac{\partial S}{\partial t} + q\frac{\partial S}{\partial x} = 0 \qquad (2.18)$$

Multiplying (2.16) by $\frac{a}{\rho}$ and (2.18) by $\frac{1}{a\rho}\left(\frac{\partial p}{\partial S}\right)_\rho$ and adding,

$$\frac{1}{a\rho}\left(\frac{\partial p}{\partial t} + q\frac{\partial p}{\partial x}\right) + a\frac{\partial q}{\partial x} = 0 \qquad (2.19)$$

Now, from (2.1 and (2.19),

$$dq \pm \frac{1}{a\rho}dp = \left(\frac{\partial q}{\partial t} \pm \frac{1}{a\rho}\frac{\partial p}{\partial t}\right)dt + \left(\frac{\partial q}{\partial x} \pm \frac{1}{a\rho}\frac{\partial p}{\partial x}\right)dx$$

$$= (dx - (q \pm a)\,dt)\left(\frac{\partial q}{\partial x} \pm \frac{1}{a\rho}\frac{\partial p}{\partial x}\right) \qquad (2.20)$$

Therefore, if a wave satisfies the direction conditions,

$$\frac{dx}{dt} = q \pm a \tag{2.21}$$

then

$$\frac{dq}{dp} = \mp \frac{1}{a\rho} \tag{2.22}$$

(For a perfect gas this may be integrated to give the well known relation $q \pm \frac{2}{\gamma-1} a = \text{constant}$).

Equation (2.22) may be integrated for a real gas by a similar process described for the integration of equation (2.2) in Section 2.11. An example is shown in Fig.4 for the unsteady expansion of air from 300°K and 100 atmospheres. It can be seen from Figure 4.5 that for a given pressure ratio, the real gas attains a higher flow velocity than the perfect gas.

In Figure 4.6, the flow velocity (q) is plotted against speed of sound (a). A check on the accuracy of the calculations is provided by these curves as the perfect gas should obey the condition of invariance of the Riemann variable $\left(\frac{2}{\gamma-1} a + q\right)$. It may be seen from Figure 4.6 that the real gas departs widely from this condition and, as most practical problems are solved by using Riemann's variables, large errors would be introduced by the assumption of a perfect gas in this example, in which relatively moderate temperature and pressures are considered.

2.2 Shock waves

The flow through a normal shock wave is described by the equations of continuity, momentum and energy. The conventional normal shock wave relations for a perfect gas are obtained by replacing the enthalpy term in the energy equation by $\frac{\gamma}{\gamma-1} \frac{p}{\rho}$ which enables the pressure, temperature, density and velocity ratios across the shock front to be found as functions of M_1 and γ. In the case of a real gas, however, enthalpy must be left in the energy equations, as such, and the equations are then solved by making use of the real gas values of specific enthalpy which are tabulated as functions of temperature and pressure in references 4 and 5.

It can easily be seen from momentum considerations that the tangential component of the flow velocity is the same on both sides of an oblique shock wave. The equations of continuity, momentum and energy, when written in terms of the normal velocity components, are then identical with those for a normal shock wave. Therefore, for any flow geometry, the oblique shock wave problem reduces to that of finding the strength of the "equivalent normal shock wave" and this may be done by trigonometrical considerations.

2.21 Normal shock waves

The continuity, momentum and energy equations may be written,

$$\rho_1 q_1 = \rho_2 q_2 \tag{2.23}$$

$$p_1 + \rho_1 q_1^2 = p_2 + \rho_2 q_2^2 \tag{2.24}$$

and

$$\frac{q_1^2}{2} + H_1 = \frac{q_2^2}{2} + H_2 \tag{2.25}$$

From, (2.23) and (2.24),

$$p_2 - p_1 = \rho_1^2 q_1^2 \left(\frac{1}{\rho_1} - \frac{1}{\rho_2}\right) \tag{2.26}$$

also

$$\tfrac{1}{2}(q_1^2 - q_2^2) = \tfrac{1}{2}\rho_1^2 q_1^2 \left(\frac{1}{\rho_1^2} - \frac{1}{\rho_2^2}\right) \tag{2.27}$$

From (2.25) and (2.27),

$$H_2 - H_1 = \tfrac{1}{2}(p_2 - p_1)\left(\frac{1}{\rho_2} + \frac{1}{\rho_1}\right) \tag{2.28}$$

The following procedure is adopted to solve this equation when the gas in front of the shock wave is at a known temperature and pressure.

(i) Find H_1, a_1 and ρ_1 from the thermodynamic tables of real gases.

(ii) Choose a value of T_2.

(iii) Use the real gas tables to find the value of H_2 at this temperature for a number of values of p_2 and plot $H_2 - H_1$ against p_2 as shown in Fig.5.2.

(iv) Find ρ_2 from the tables for the same range of values of p_2 and evaluate $\frac{1}{2}(p_2 - p_1)\left(\frac{1}{\rho_2} + \frac{1}{\rho_1}\right)$ in each case. The curve of $\frac{1}{2}(p_2 - p_1)\left(\frac{1}{\rho_2} + \frac{1}{\rho_1}\right)$ against p_2 may be plotted on the same axes as that of $H_2 - H_1$ against p_2 and the intersection of the two curves gives the value of p_2 which corresponds to the chosen value of T_2. (See Fig.5.2).

(v) The corresponding values of ρ_2 and a_2 may then be found from the tables.

The procedure is repeated for other values of T_2 and consistent sets of values of the ratios $\frac{T_2}{T_1}, \frac{p_2}{p_1}, \frac{\rho_2}{\rho_1}, \frac{q_2}{q_1}$ and $\frac{a_2}{a_1}$ are thus found. The next step is to find the value of shock Mach number to which each of these sets corresponds. This is easily done as, by (2.26),

$$M_S^2 = M_1^2 = \frac{q_1^2}{a_1^2} = \frac{1}{a_1^2} \cdot \frac{p_2 - p_1}{\rho_1^2\left(\frac{1}{\rho_1} - \frac{1}{\rho_2}\right)}$$

i.e.

$$M_S^2 = \frac{1}{a_1^2} \cdot \frac{p_1}{\rho_1} \frac{\left(\frac{p_2}{p_1} - 1\right)}{\left(1 - \frac{\rho_1}{\rho_2}\right)} \tag{2.29}$$

It is often required to find the flow velocity behind a normal shock wave moving into a gas at rest. This is given by,

$$U_2 = q_1 - q_2$$

and using (2.23)

$$= q_1 \left(1 - \frac{\rho_1}{\rho_2}\right)$$

i.e.

$$U_2 = a_1 M_S \left(1 - \frac{\rho_1}{\rho_2}\right) \qquad (2.30)$$

The method of solution is shown in Fig.5.2 for three values of T_2 for air initially at 300°K and 0.1 atm. The calculations were also carried out for a number of other values of T_2 and also for air initially at 0.01 atm and 300°K. The shock Mach number to which each of these solutions corresponds was found from equation 2.29 and Figures 5.3 to 5.6 show the departures from the perfect gas values of pressure, temperature, density and velocity ratios across the shock and of the flow Mach number behind a shock moving into a gas at rest.

The pressure ratio (Figure 5.3) across the shock is greater for the real gas than for the perfect gas and there is no significant dependence on pressure in the example which has been considered. The temperature ratio (Figure 5.4) for the real gas is far lower than that for the perfect gas and at high shock Mach numbers, when dissociation is the dominant factor, the effect is greater for the gas initially at the lower pressure. However, there is still an appreciable effect at shock Mach numbers around five and, at these speeds, thermal imperfections cause the effect to be slightly greater for the gas initially at the higher pressure. Figure 5.5 shows that the density is higher behind a shock in the real gas and the steady flow velocity is less. According to the perfect gas theory, the maximum flow Mach number behind an unsteady normal shock wave in a gas of $\gamma = 1.4$ is 1.89 but Figure 5.6 shows that the flow Mach number in a real gas may be very much higher.

The above results are merely given to illustrate the method and the variation of these and other quantities for different initial conditions may be easily calculated.

2.22 Oblique shock waves

The equation of continuity gives

$$\rho_1 u_1 = \rho_2 u_2 \qquad (2.31)$$

The equation of momentum may be applied to flow normally and tangentially to the wave front to give

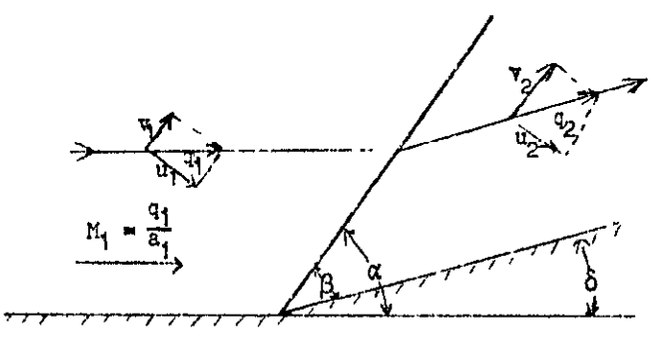

$$p_1 - p_2 = \rho_2 u_2^2 - \rho_1 u_1^2 \qquad (2.32)$$

and $$0 = \rho_2 u_2 v_2 - \rho_1 u_1 v_1 \qquad (2.33)$$

Comparing (2.31) with (2.33) it is seen that

$$v_1 = v_2 = v \qquad (2.34)$$

The energy equation may therefore be written

$$\frac{u_1^2 - u_2^2}{2} = \frac{q_1^2 - q_2^2}{2} = H_2 - H_1 \qquad (2.35)$$

Hence the equations in u_1 and u_2 for the oblique shock wave are identical to those in q_1 and q_2 for the normal shock wave.

Let $M_S = \frac{u_1}{a_1}$ be the "equivalent normal shock" Mach number.

Now $$\tan\beta = \tan(\alpha - \delta) = \frac{\tan\alpha - \tan\delta}{1 + \tan\alpha \tan\delta}$$

But $$\tan\beta = \frac{u_2}{v} \quad \text{and} \quad \tan\alpha = \frac{u_1}{v}$$

$$\therefore \quad \frac{u_2}{v} = \frac{\frac{u_1}{v} - \tan\delta}{1 + \frac{u_1}{v}\tan\delta}$$

$$\therefore \quad \frac{u_2}{u_1} = \frac{1 - \tan\delta \frac{v}{u_1}}{1 + \frac{u_1}{v}\tan\delta}$$

But, $$\frac{v}{u_1} = \sqrt{\frac{q_1^2 - u_1^2}{u_1^2}} = \sqrt{\frac{q_1^2}{a_1^2} \cdot \frac{a_1^2}{u_1^2} - 1} = \sqrt{\frac{M_1^2}{M_S^2} - 1}$$

Therefore,

$$\frac{u_2}{u_1} = \frac{1 - \tan\delta \sqrt{\frac{M_1^2}{M_S^2} - 1}}{1 + \frac{\tan\delta}{\sqrt{\frac{M_1^2}{M_S^2} - 1}}} \qquad (2.36)$$

Equation (2.36) enables the "equivalent normal shock" Mach number to be plotted as a function of $\frac{u_2}{u_1}$ for any given flow Mach number and deflection angle. (Note that the value of $\frac{u_2}{u_1}$ depends only on the ratio of M_1 to M_S and not on their individual values so that, after one curve has been

calculated, the others for the same value of δ are simply scaled from it). These curves are based solely on geometrical considerations and hold for real or perfect gases.

The shock wave equations must also be satisfied and curves of $\frac{u_2}{u_1}$ against M_S which do this may be obtained using the methods of section 2.21. (As $\frac{u_2}{u_1}$ for the oblique shock is equal to $\frac{q_2}{q_1}$ for the equivalent normal shock). Examples of the two sets of curves are plotted in Figure 6.1 and their points of intersection give the appropriate values of the equivalent normal shock Mach number for the given flow Mach number deflection angle and initial gas conditions. There are, in general, two solutions for each case, the first corresponds to the "weak" shock which is the one normally observed and the second corresponds to the "strong" shock. When the curves do not intersect the shock wave becomes detached.

The angle of inclination α of the shock wave is given by,

$$\sin\alpha = \frac{u_1}{q_1} = \frac{M_S}{M_1} \qquad (2.37)$$

As this relation is a function only of the ratio $\frac{M_1}{M_S}$, the family of curves which it gives are easily constructed (Figure 6.2).

Figure 6.3 has been constructed from Figures 6.1 and 6.2 and gives the shock wave angle as a function of M_1 for various values of deflection angle for the real and perfect gas cases. It is seen that the angle of the "weak" shock is less for the real gas than for the perfect gas. Also, at any given Mach number, the shock wave remains attached until higher values of deflection angle have been attained in the real gas than in the perfect gas. For instance, there is no solution at all at a deflection angle of 50° for the perfect gas but the shock is attached above $M_1 = 8$ for the real gas.

Once the value of the "equivalent normal shock" Mach number has been found from Figure 6.1, the normal shock wave calculations (Section 2.21) give the ratios of pressure, density etc. across the oblique shock wave. The pressure ratio across the shock is plotted in Figure 7.1 and, for a given initial Mach number and flow deflection angle, the pressure rise is less for the real gas than for the perfect gas.

The flow Mach number behind the shock is often required and is given by,

$$M_2 = \frac{q_2}{a_2} = \frac{a_1}{a_2} \cdot \frac{u_1}{a_1} \cdot \frac{q_2}{u_1},$$

$$= M_S \cdot \frac{a_1}{a_2} \sqrt{\frac{u_2^2}{u_1^2} + \frac{v^2}{u_1^2}}$$

i.e.
$$M_2 = M_S \cdot \frac{a_1}{a_2} \cdot \sqrt{\left(\frac{u_2}{u_1}\right)^2 + \left(\frac{M_1^2}{M_S^2} - 1\right)} \qquad (2.38)$$

For a given value of M_1 and δ, M_S and $\frac{u_2}{u_1}$ are found from Figure 6.1 and the corresponding value of $\frac{a_1}{a_2}$ is given by the normal shock wave calculations. The Mach number behind the shock is greater for the real gas than for the perfect gas. (Figure 7.2).

3 Application of Methods to Typical Problems

3.1 Shock tube performance

The general principles of operation of shock tubes are well known, A tube is divided by a diaphragm into two sections, one containing gas at high pressure and the other at low pressure. The diaphragm is ruptured and the gas in the high pressure section expands isentropically into the low pressure section. The gas in the low pressure section is compressed by a shock wave which travels into it. The gas which was originally in the high pressure section is divided from that which was originally in the low pressure section by a contact surface which also travels into the low pressure section.

The values of pressure and velocity are the same on each side of the contact surface and this provides the basis of a simple graphical method (see Figure 8) for calculating the performance of a shock tube for both the perfect and real gas cases. The methods of section 2.13 enable curves to be constructed of flow velocity (q) against pressure (p) in the expanded high pressure gas. These are shown in Fig.8 for both air and hydrogen expanded from 100 atmospheres and 300°K. The methods of section 2.21 may then be used to construct curves of flow velocity behind an unsteady normal shock wave (U_2) against pressure behind the shock (p_2). These are shown in Figure 8 for air compressed from 0.1 atmospheres and 300°K. All these curves are drawn for both the real and perfect gas cases.

As flow velocity and pressure are continuous across the contact surface, the intersections of these two families of curves give solutions of the shock tube problem. For instance, points (A) and (B) in Figure 8 give respectively the perfect and real gas solution for the flow velocity and pressure at the contact surface of a shock tube having hydrogen at 100 atmospheres and 300°K in the high pressure end and air at 0.1 atmospheres and 300 °K in the low pressure end. In order to find the strength of the shock wave which is produced, the methods of section 2.21 are again used to find the relation between shock Mach number (M_S) and the flow velocity (U_2) behind it. This is different for the real and perfect gas cases and a scale of M_S, for the two cases, has been added to Figure 8. It may be seen from this that point (A) corresponds to a shock Mach number of 7.39 and point (B) corresponds to one of 7.06.

Figures 9.1 and 9.2 have been constructed solely from the information given directly by curves of the type shown in Figure 8 and show the reduction in shock Mach number which is produced by the real gas effects. The magnitude of the effects varies with the pressure of the high pressure gas as a result of thermal imperfections becoming apparent at the higher pressures. One of the advantages of this graphical method is that it may be seen, in any particular case, to what extent the reduction in shock Mach number is due to effects in the expansion of the high pressure gas (mainly thermal imperfections) and what is due to effects in the compression of the low pressure gas (mainly caloric imperfections). In particular, it is seen that considerable effects are produced with air as the high pressure gas at 100 atmospheres even when the shock Mach number is only two or three (see Figure 9.2). Also, if the high pressure gas is such that the imperfections in its expansion are negligible, it may be seen from Figure 8 that the velocity of the contact surface may be increased even though the shock Mach number is reduced. In any case, when the shock velocity is high, the velocity of the contact surface

is not reduced as much as the shock front and so, at any point down the tube, the interval between the arrival of the shock wave and contact surface is reduced. As the gas between the shock wave and contact surface is used for testing purposes in impulse tunnels, the real gas effects cause a reduction in the running time. The time interval between the shock wave and contact surface per unit length of tube is given by:

$$\frac{t}{x} = \left(\frac{1}{U_2} - \frac{1}{a_1 M_S}\right), \qquad (3.1)$$

and Figure 9.3 shows the reduction in running time due to imperfect gas effects in a typical case.

3.2 Lift of flat plate

An exact solution for the lift of a two-dimensional flat plate at incidence in a supersonic stream may be found by calculating the drop in pressure over the upper surface through the Prandtl-Meyer expansion and the increase in pressure over the lower surface through the oblique shock wave. The lift coefficient of a flat plate is shown in Figure 10 for incidences of up to 40° and at Mach numbers of 5, 10 and 15 in air at 300°K and 0.01 atmospheres.

The Prandtl-Meyer expansion is treated in Section 2.12 but, for the initial conditions of this example, the imperfect gas effects on the expansion will be negligible. The main factor will be the pressure rise through the oblique shock wave and this is shown in Figure 7.1 for the real and perfect gas cases. The pressure rise is less for the real gas so that the lift coefficient will be reduced from that given by perfect gas theory.

3.3 Nozzle of hypersonic impulse tunnel

The Mach number of the steady flow behind an unsteady normal shock wave is limited to quite low values and, in order to produce higher Mach numbers, the flow is often expanded in a supersonic nozzle. Figure 11 shows the nozzle profile which would be required to produce a steady flow of Mach 6 at the end of a shock tube in which a shock of Mach number 12 is produced in air initially at 300°K and 0.5 atmospheres. The inlet Mach number is higher for the real gas than for the perfect gas (see Figure 5.6).

The Prandtl-Meyer angle was found for the real gas by the same methods as those used to produce Figure 3.4. A sinusoidal distribution of Mach number was chosen along the centre line and the methods of characteristics was used to construct the flow field. The nozzle profile was found as a streamline of this flow. It would be expected from Figure 1.8 that the overall area ratio would be much higher for the real gas than for the perfect gas and this has been borne out in this example. As this example involves reassociation of the initially dissociated gas, the neglect of non-equilibrium effects may be serious.

3.4 Reflection of normal shock wave from rigid wall

Consider an unsteady normal shock wave moving in a one-dimensional channel which has a closed end. When the shock wave meets the end it is reflected and the strength of the reflected wave is determined by the condition of zero flow adjacent to the wall. The change in velocity across each wave must therefore be the same (i.e. $|\Delta q|_R = |\Delta q|_I$). For a perfect gas, $\frac{|\Delta q|_I}{a_2}$ is a function of M_{S_I} only and $\frac{|\Delta q|_R}{a_2}$ is a function of

M_{S_R} only and they may be plotted as shown in Figure 12.2. In the case of a real gas, $\frac{|\Delta q|_R}{a_2}$ depends on M_{S_I} as well as M_{S_R} and has been plotted in Figure 12.2. For several values of M_{S_I}. To find the value of M_{S_R} for any value of M_{S_I}, the value of $\frac{|\Delta q|_I}{a_2}$ is found for M_{S_I} and the required value of M_{S_R} is that which gives $\frac{|\Delta q|_R}{a_2} = \frac{|\Delta q|_I}{a_2}$. The process is illustrated in Figure 12.2 for $M_{S_I} = 8.0$ for the real and perfect gas cases, giving $M_{S_R} = 2.89$ and 2.55 respectively. The real gas curves have all been calculated by the methods described in Section 2.21.

The Mach number of the reflected shock is plotted as a function of the Mach number of the incident shock in Figure 12.3 and it is seen that, whereas the Mach number of the reflected shock is asymptotic to a value of 2.63 for a perfect gas, it may be much higher for a real gas. Figure 12.4 shows that the temperature ratio across the reflected shock is much less for the real gas than for the perfect gas. The ratio of the temperature adjacent to the wall before and after the arrival of the shock is shown in Fig. 12.5 and is again considerably less for the real gas. However, it is seen from Figure 12.6 that the pressure ratio is greater for the real gas and, for incident shock Mach numbers above about 8, the difference is very significant.

3.5 Two-dimensional supersonic intake

A two-dimensional intake may be designed in which a uniform supersonic stream is compressed by two oblique shock waves to form another uniform stream in the same direction at a much lower Mach number. The general configuration is shown in Figure 13.1 for a perfect gas of $\gamma = 1.4$ and for air initially at 300°K and 0.01 atmospheres at intake Mach numbers of 6, 10 and 14. An oblique shock wave is formed when the stream is turned through an angle of 30° and the stream is returned to its original direction by the reflected oblique shock wave. At an intake Mach number of 6, a solution is possible with regular reflection for the real gas but Mach reflection occurs in the perfect gas case.

The properties of the incident oblique shock may be found for the perfect and real gas cases from the graphs in Figures 6 and 7. These also enable the reflected oblique shock properties to be found for the perfect gas but, to obtain the solution for the real gas, similar curves must be constructed for initial temperatures and pressures corresponding to those behind the incident shock.

Figures 13.2 to 13.5 show the variation with intake Mach number of the temperature and area ratios and the exit Mach number and total pressure. It is seen that the real gas intake provides a narrower stream of air at a lower temperature but at a higher Mach number and total pressure than that for the perfect gas.

List of Symbols

p pressure

ρ density

T temperature

R universal gas constant

S	entropy
H	enthalpy
m	molecular weight
C_p	specific heat at constant pressure
C_v	specific heat at constant volume
$\gamma = \frac{C_p}{C_v}$	specific heat ratio
q	flow velocity
x	linear coordinate
r	radial coordinate
θ	angular coordinate
t	time
u	radial flow velocity component in Prandtl-Meyer expansion or normal flow velocity component through oblique shock wave
v	tangential velocity component
a	local velocity of sound
$M = \frac{q}{a}$	flow Mach number
M_S	normal shock Mach number
U_2	absolute flow velocity behind unsteady normal shock wave
A	cross-sectional area
ν	flow deflection angle (Prandtl-Meyer angle)
α	angle between oblique shock wave and original flow direction
β	angle between oblique shock wave and final flow direction
δ	flow deflection angle through oblique shock wave

Superscript

$*$	sonic conditions

Subscripts

o	stagnation conditions
1	conditions in front of shock wave
2	conditions behind shock wave
3	conditions behind reflected shock wave

REFERENCES

No.	Author	Title, etc.
1	Tsien, H.S.	One-dimensional flows of a gas characterised by van der Waal's equation of state Vol. 25, No.6, pp.301-324, 1947 Journ. of Mathematics and Physics
2	Eggers, A.J.	One-dimensional flow of an imperfect diatomic gas NACA Tech Note No. 1861, 1949
3	Tao, L.N.	Gas dynamic behaviour of real gases Vol. 22, No. 11, pp.763-774, Nov. 1955 Journ. of Aeronautical Sciences
4	Staff of App. Phys. Lab., J.H.U.	Handbook of supersonic aerodynamics (NAVORD Report No. 1488). Vol. 5, Sect. 15. Properties of gases
5	Hilsenrath, J. et al.	Tables of thermal properties of gases National Bureau of Standards, Circular 564. November, 1955
6	Hilsenrath, J, and Beckett, C.W.	Thermodynamic properties of argon - free air (0.78847 N_2, 0.21153 O_2) to 15000°K National Bureau of Standards, Report No. 3991, April, 1955
7	Zienkiewicz, H.K.	On some problems in one-dimensional flow of imperfect gases English Electric Co. Ltd., Report No. L.A.m. 082. March 1955
8	Squire, W., Hertzberg, A., and Smith, W.E.	Real gas effects in a hypersonic shock tunnel Arnold Engineering Development Centre Report No. AEDC-TN-55-14. March 1955
9	Romig, M.F.	The normal shock properties for air in dissociation equilibrium Vol. 22, No. 4, April 1955 Journ. of Aeronautical Sciences

WT.2078.C.P.397.K3 - Printed in Great Britain

FROM P_o = 100 atm, T_o = 5000 °K (AIR.)

---------- PERFECT GAS (γ = 1·4)

———— REAL GAS (THERMAL EQUILIBRIUM.)

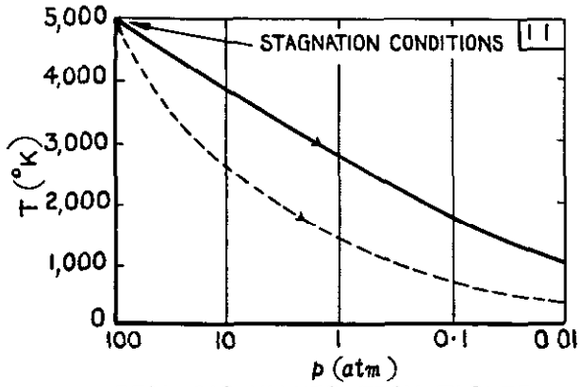

REAL GAS VALUES FROM TABLES

PERFECT GAS VALUES GIVEN BY $\frac{p}{p_o} = \left(\frac{T}{T_o}\right)^{3.5}$

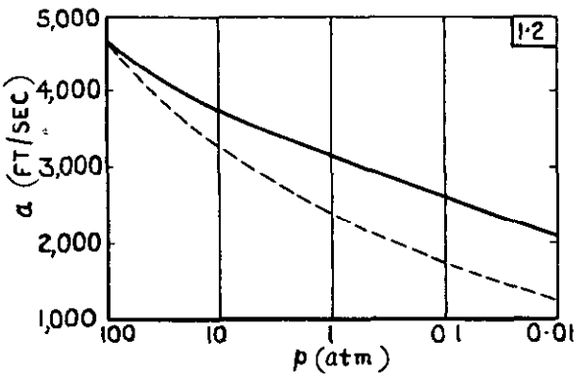

REAL GAS VALUE FROM TABLES

PERFECT GAS VALUES GIVEN BY $a = a_o\sqrt{\frac{T}{T_o}}$

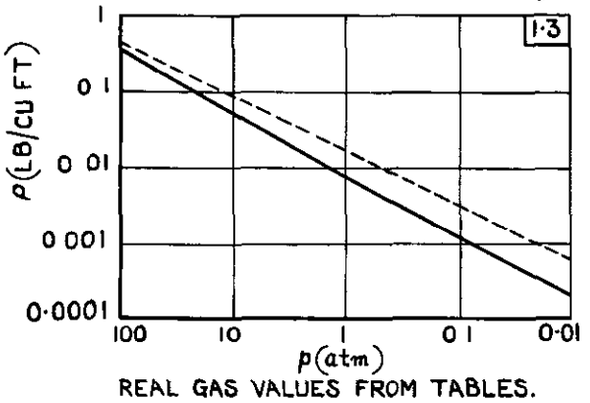

REAL GAS VALUES FROM TABLES.

PERFECT GAS VALUES GIVEN BY $\rho = \frac{mp}{RT}$

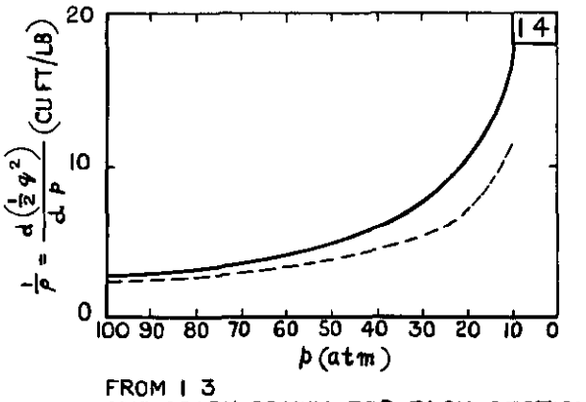

FROM 1·3

ONE GRAPH DRAWN FOR EACH SECTION OF LOGARITHMIC SCALE OF p

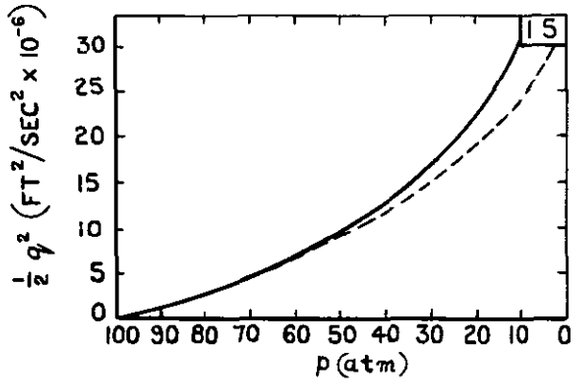

FROM 1·4 BY GRAPHICAL INTEGRATION

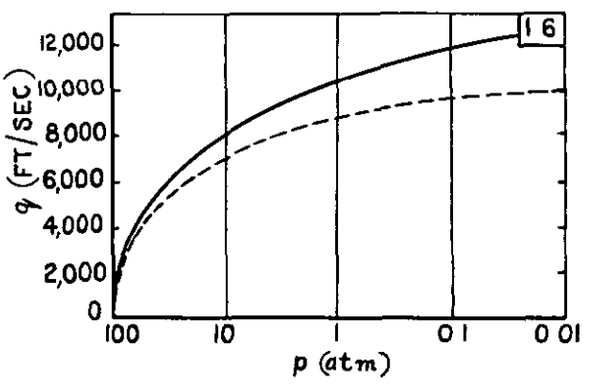

FROM 1·5.

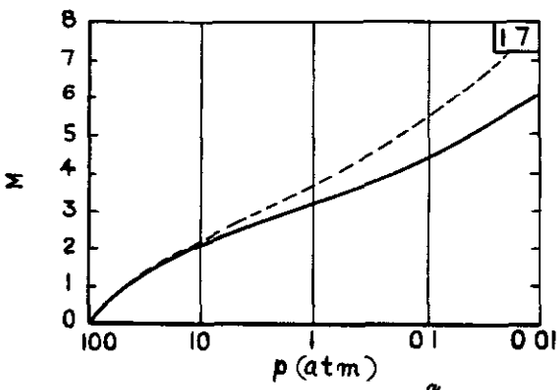

FROM 1·6 & 1·2 AS $M = \frac{q}{a}$

PERFECT GAS VALUES CHECKED BY $\frac{p}{p_o} = \left(1 + \frac{M^2}{5}\right)^{-3.5}$

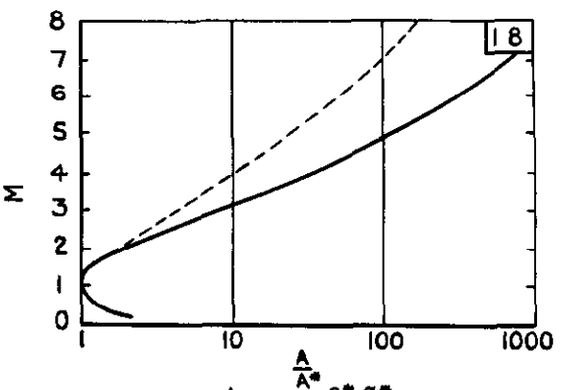

GIVEN BY $\frac{A}{A^*} = \frac{\rho^* q^*}{\rho q}$

PERFECT GAS VALUES CHECKED BY $\frac{A}{A^*} = \frac{1}{M}\left(\frac{5 + M^2}{6}\right)^3$

FIG.1. STEADY ONE-DIMENSIONAL ISENTROPIC EXPANSION.

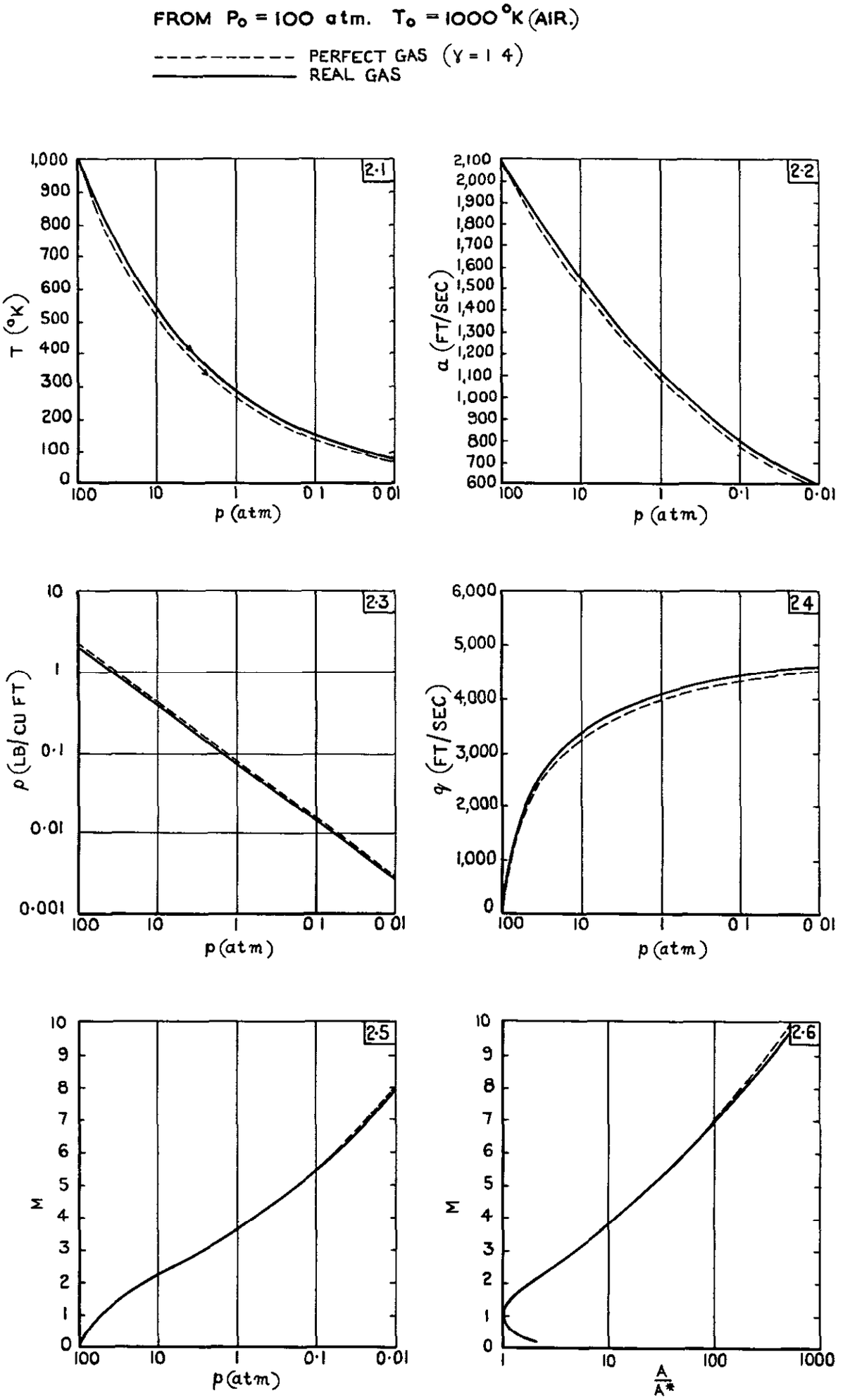

FIG.2. STEADY ONE-DIMENSIONAL ISENTROPIC EXPANSION.

FROM P_o = 100 atm , T_o = 5000 °K. (AIR)

---------- PERFECT GAS (γ = 1·4)

———— REAL GAS (THERMAL EQUILIBRIUM)

1 CONSTRUCT CURVES FOR STEADY ISENTROPIC EXPANSION. (FIG 1.)

2 TABULATE RESULTS AS FOLLOWS (ONE TABLE FOR REAL AND ONE FOR PERFECT GAS)

M	p	q	a	$\frac{1}{a} = \frac{d\theta}{d\mu}$	$\mu = \sqrt{q^2 - a^2}$
	FROM 1 7	FROM 1·6	FROM 1 2		

3 CARRY OUT FOLLOWING GRAPHICAL PROCEDURE

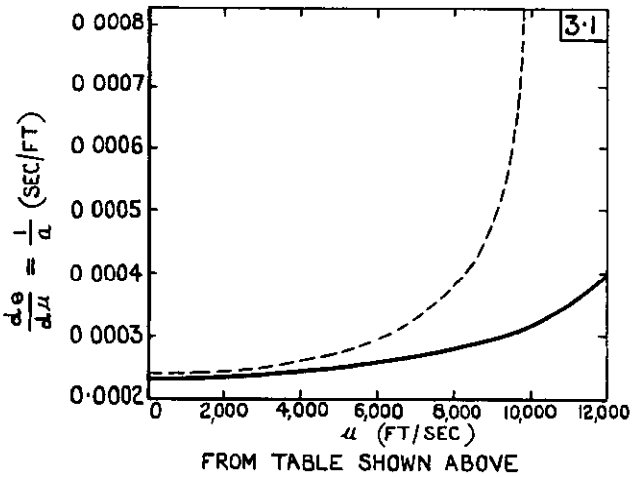

FROM TABLE SHOWN ABOVE

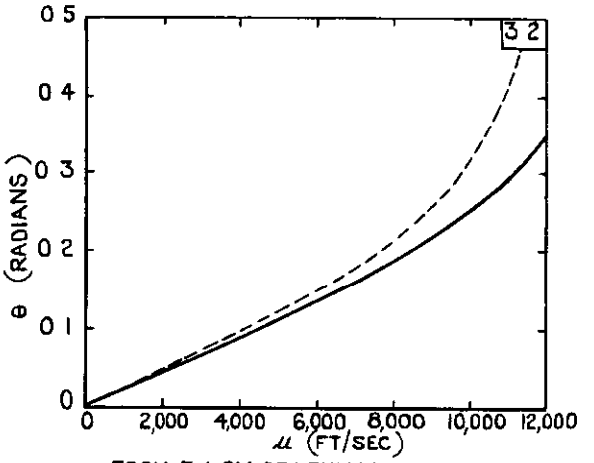

FROM 3 1 BY GRAPHICAL INTEGRATION
(NOTE - $\theta = 0$ WHEN M = 1)

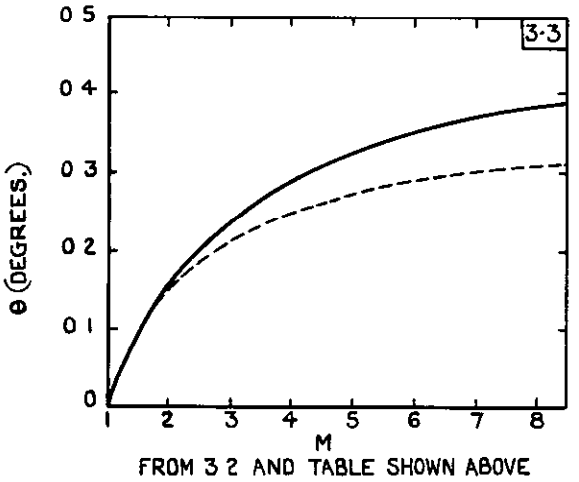

FROM 3 2 AND TABLE SHOWN ABOVE

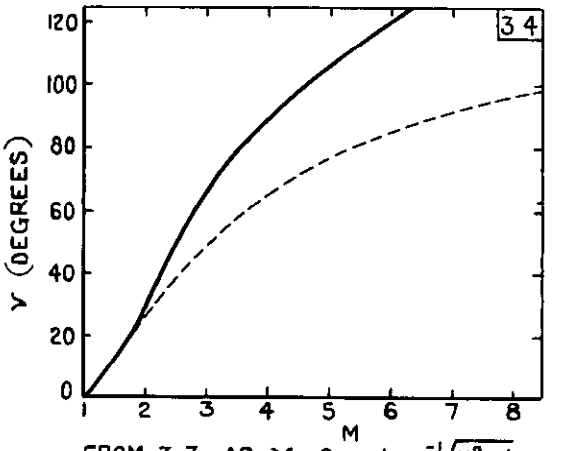

FROM 3 3 AS $\nu = \theta - \tan^{-1}\sqrt{M^2-1}$
PERFECT GAS VALUES CHECKED BY,
$\nu = \sqrt{6}\left(\tan^{-1}\sqrt{\frac{M^2-1}{6}}\right) - \tan^{-1}\sqrt{M^2-1}$

FROM P^* = 100 atm , T^* = 1000 °K (AIR)

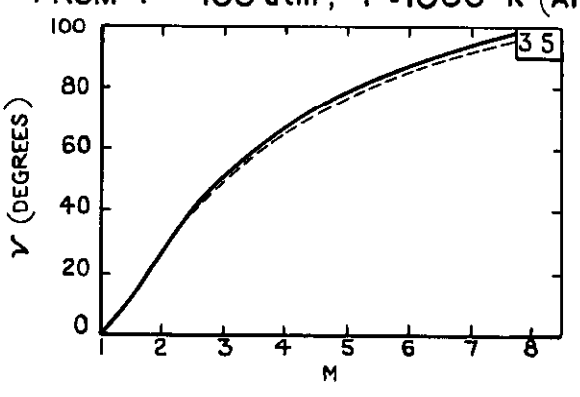

FIG.3. PRANDTL-MEYER EXPANSION ROUND CORNER.

FROM P_o = 100 atm., T_o = 300 °K (AIR.)

---------- PERFECT GAS. (γ = 1.4)

———— REAL GAS. (THERMAL EQUILIBRIUM.)

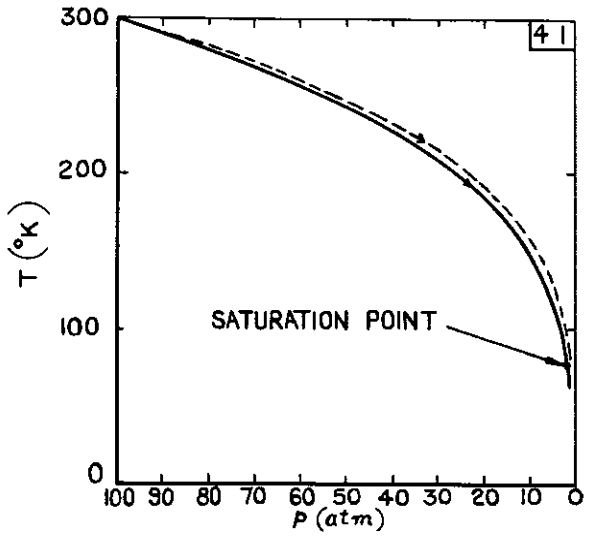

REAL GAS VALUES FROM TABLES

PERFECT GAS VALUES GIVEN BY $\frac{p}{p_o} = \left(\frac{T}{T_o}\right)^{3.5}$

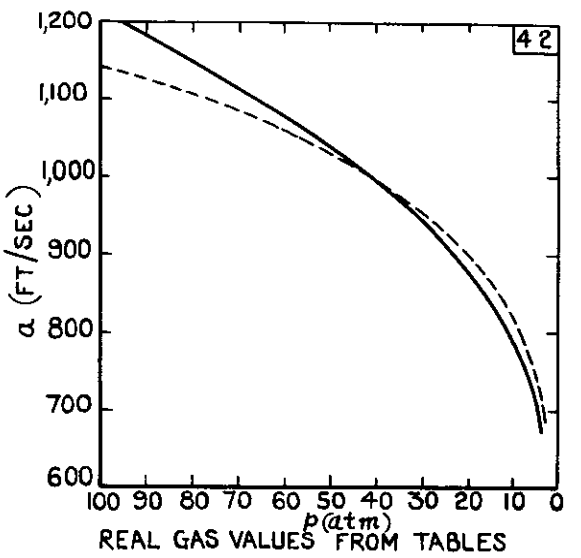

REAL GAS VALUES FROM TABLES

PERFECT GAS VALUES GIVEN BY $a = a_o\sqrt{\frac{T}{T_o}}$

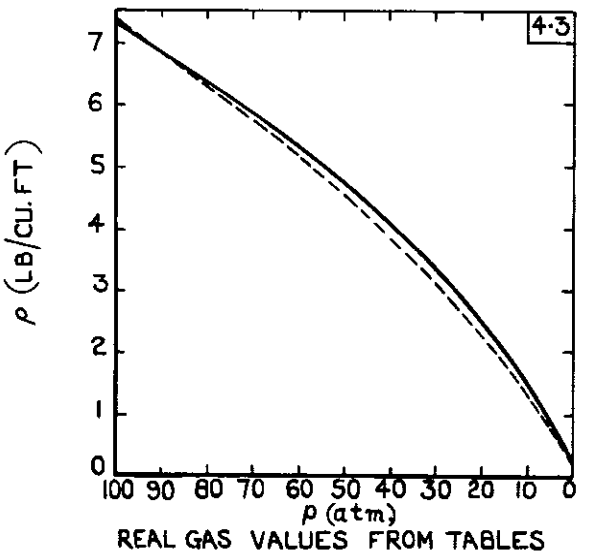

REAL GAS VALUES FROM TABLES

PERFECT GAS VALUES GIVEN BY $\rho = \frac{mp}{RT}$

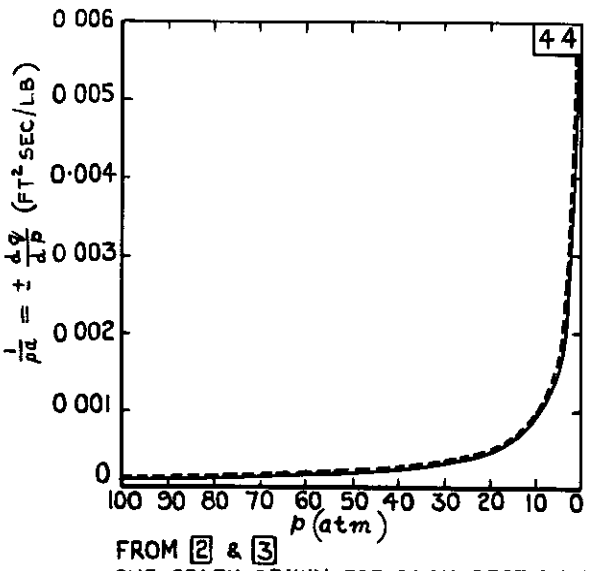

FROM [2] & [3]

ONE GRAPH DRAWN FOR EACH SECTION OF LOGARITHMIC SCALE OF p.

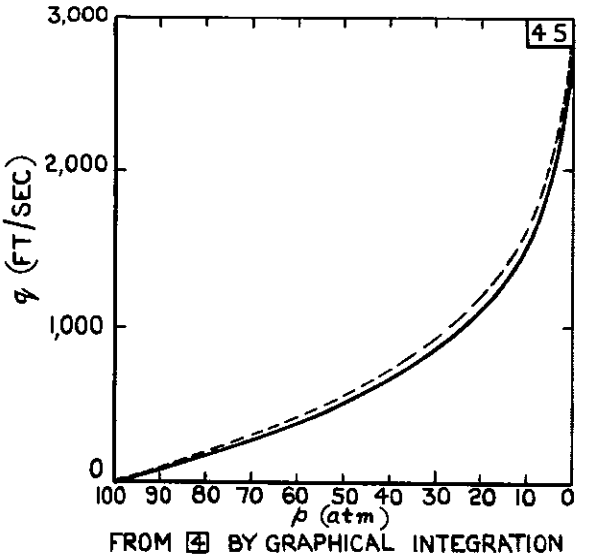

FROM [4] BY GRAPHICAL INTEGRATION

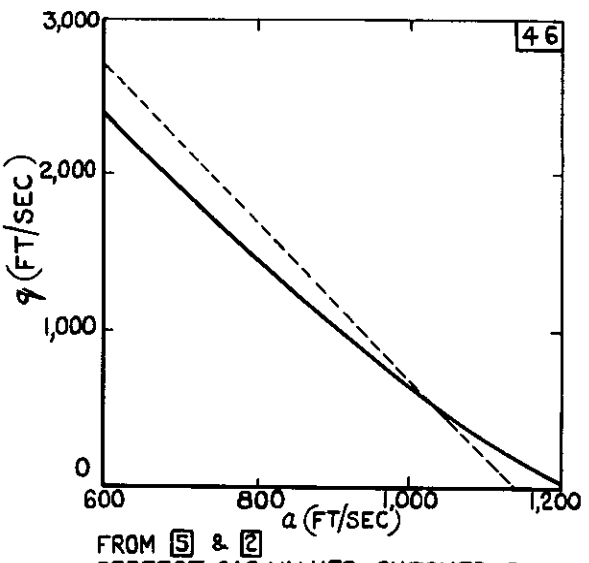

FROM [5] & [2]

PERFECT GAS VALUES CHECKED BY

$5a + q = 5a_o$

FIG. 4. PROPOGATION OF ONE-DIMENSIONAL ISENTROPIC WAVE. (UNSTEADY EXPANSION.)

FIG. 5 1.

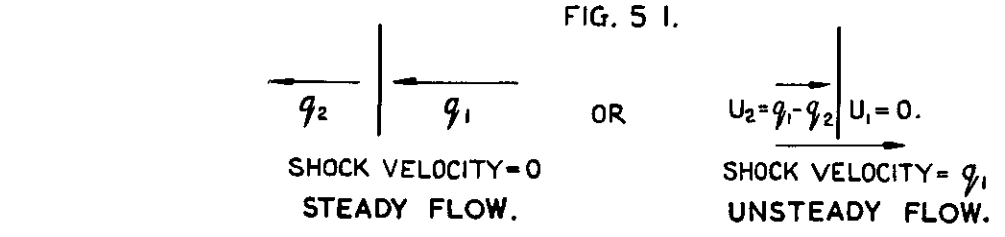

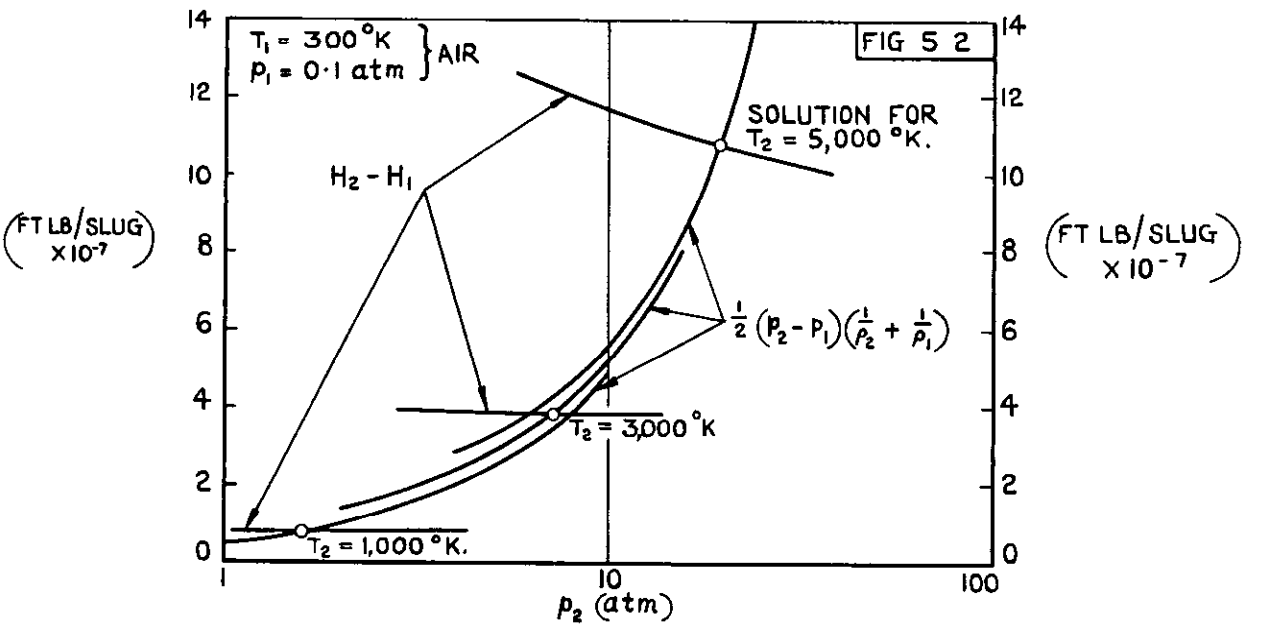

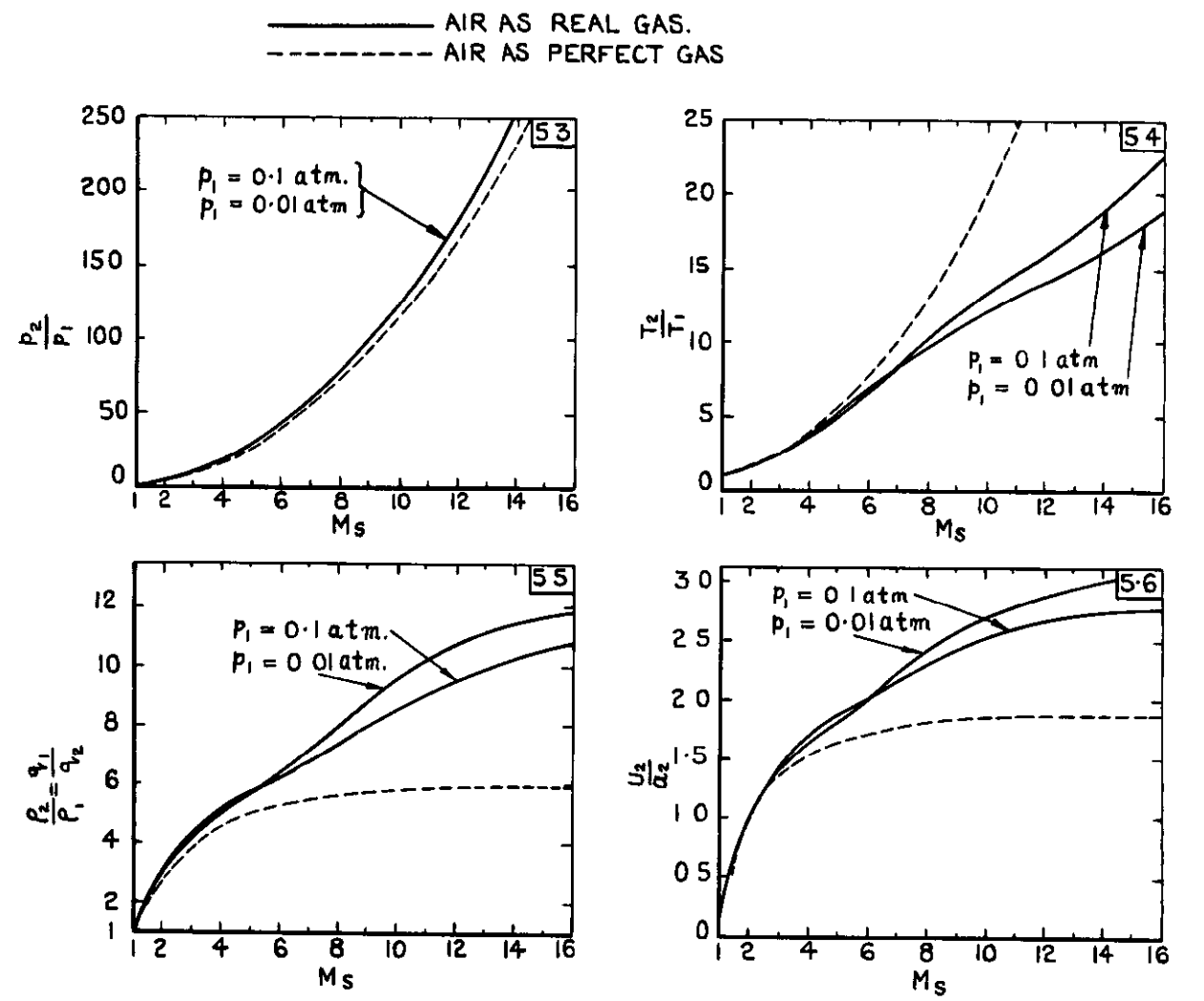

FIG. 5. NORMAL SHOCK WAVES.

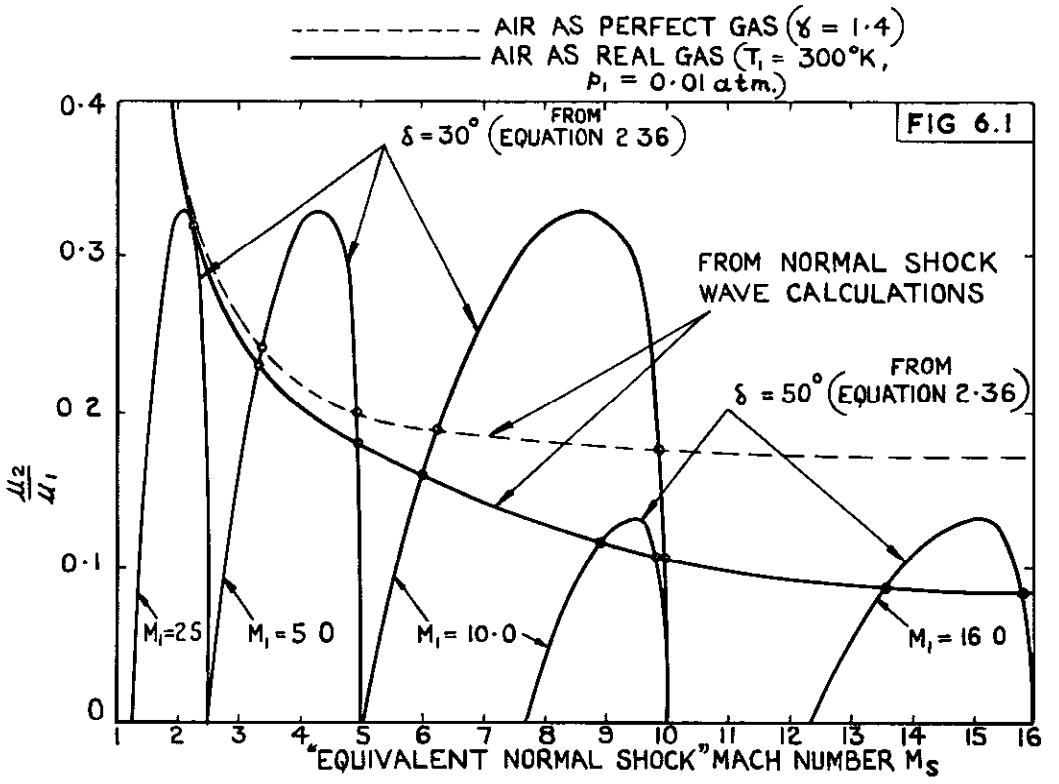

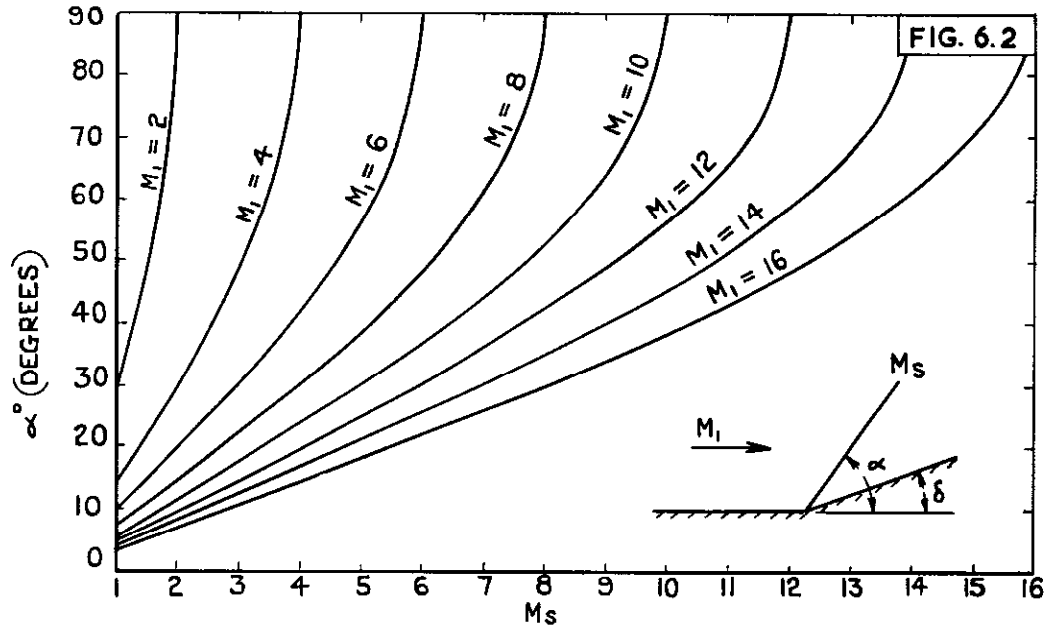

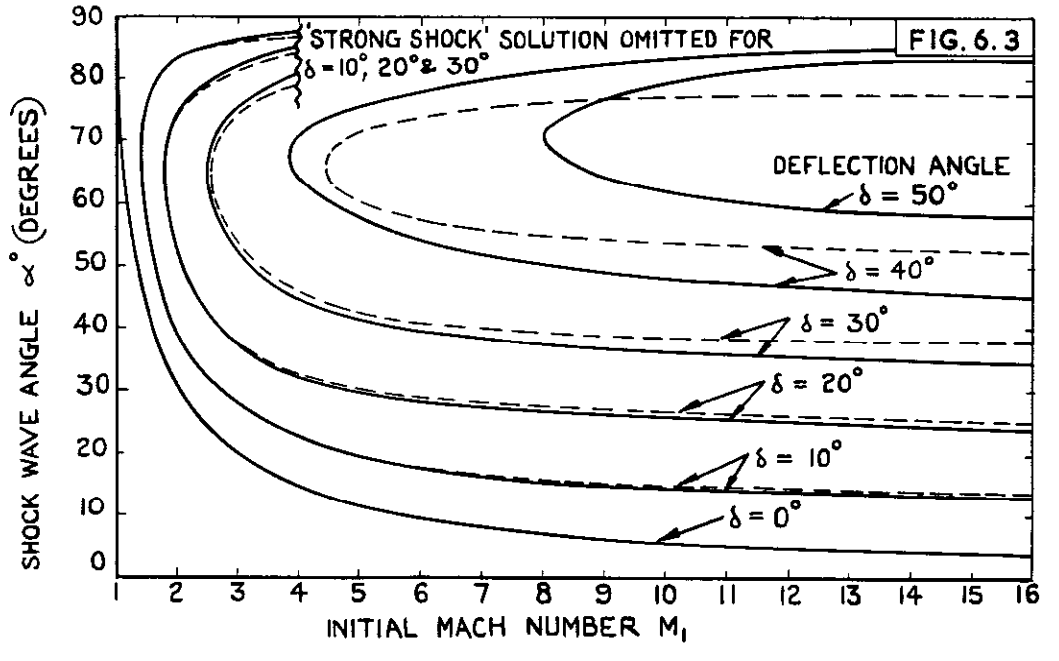

FIG. 6. OBLIQUE SHOCK WAVES.

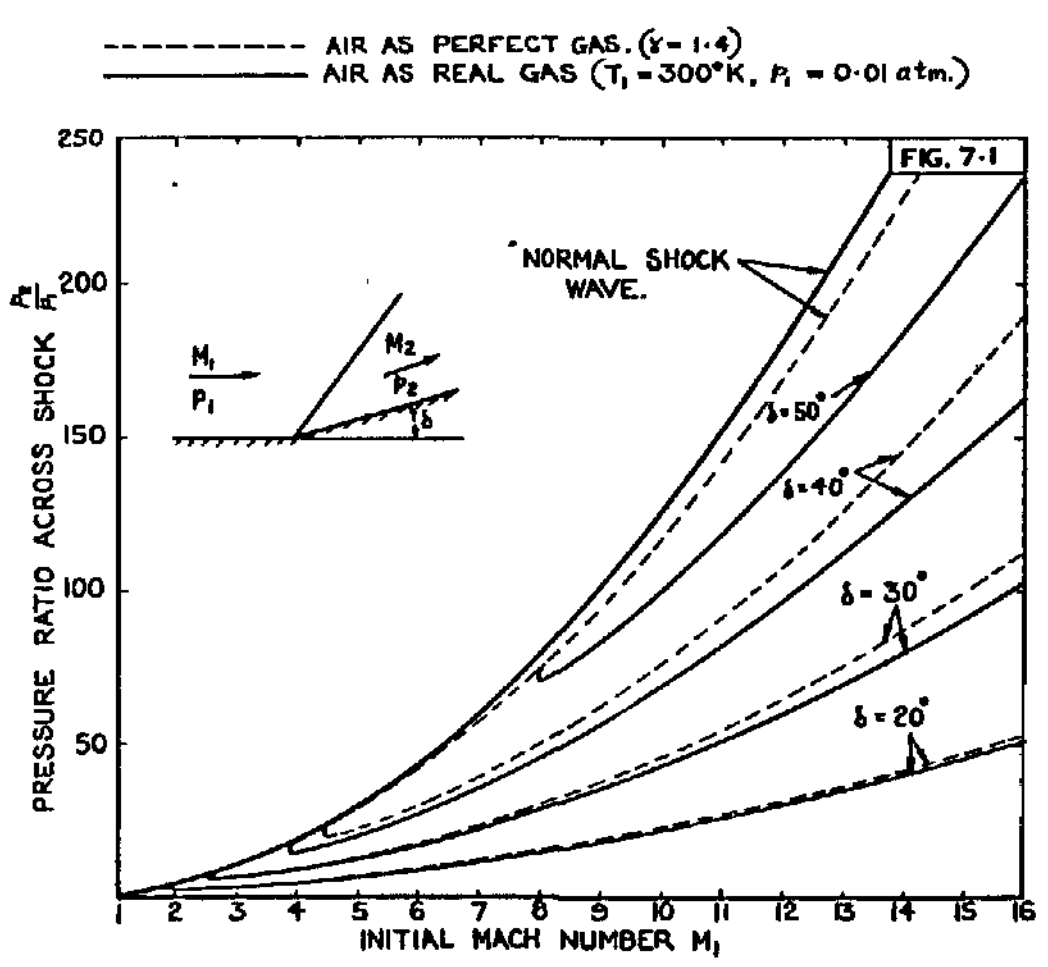

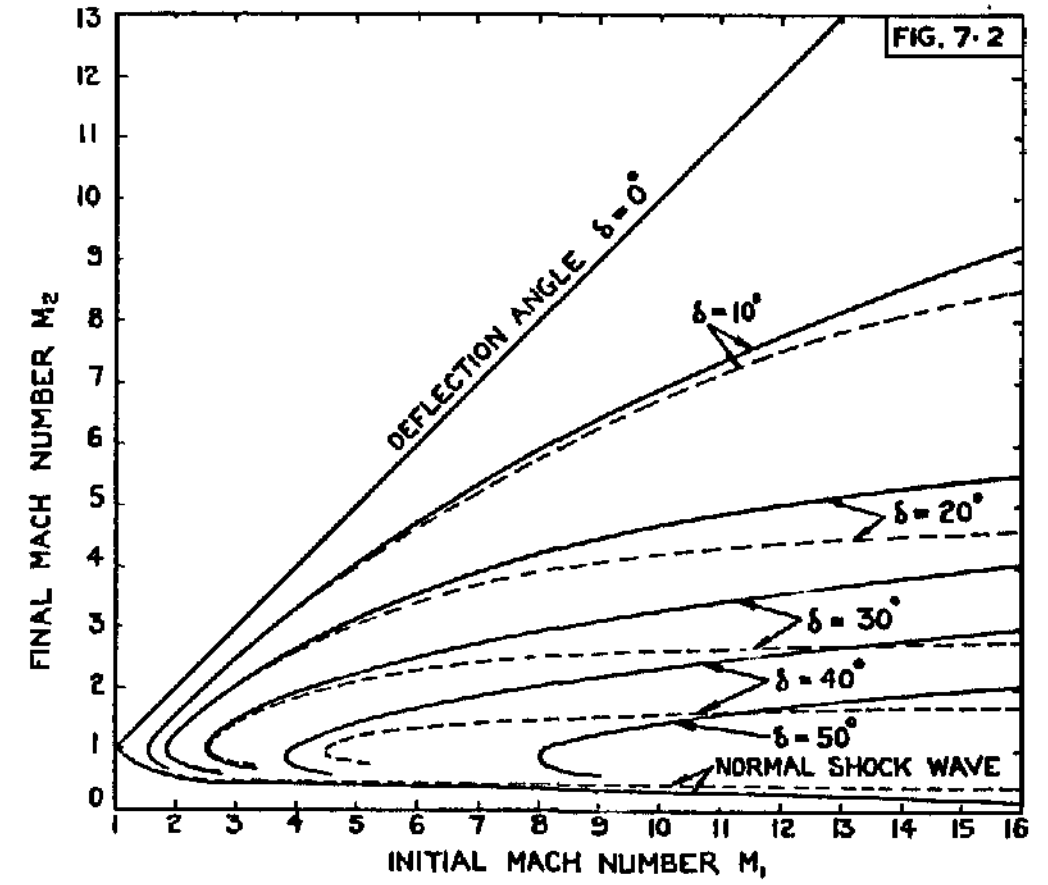

FIG. 7. OBLIQUE SHOCK WAVES.

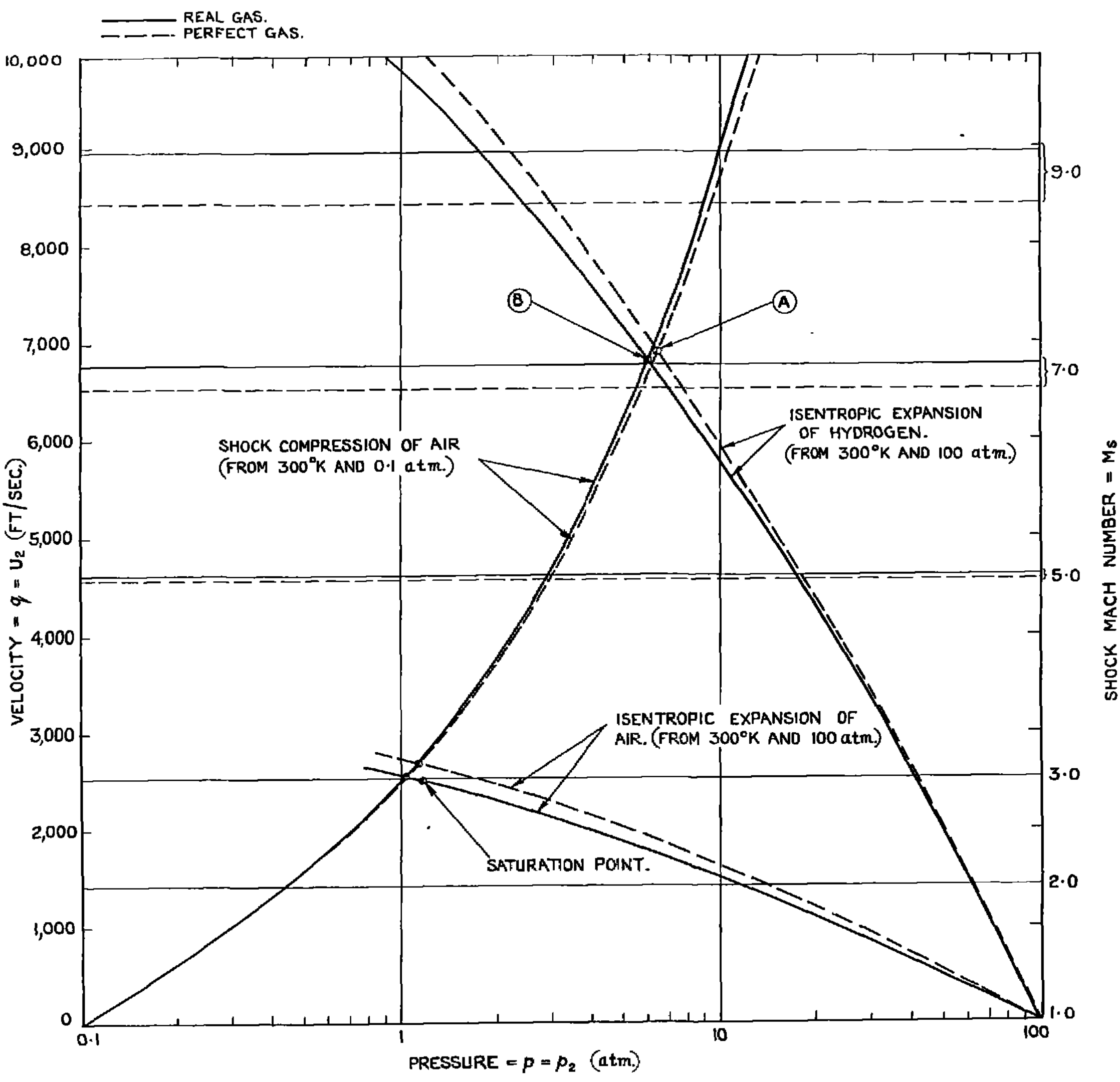

FIG. 8. IMPERFECT GAS EFFECTS ON SHOCK TUBE PERFORMANCE.

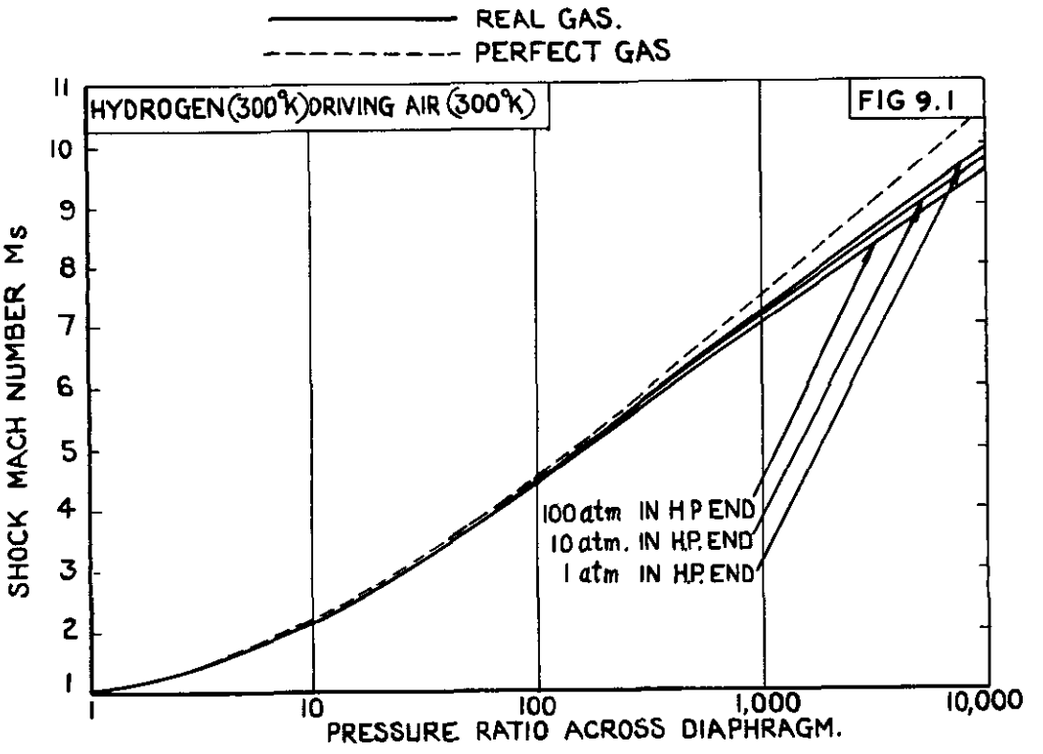

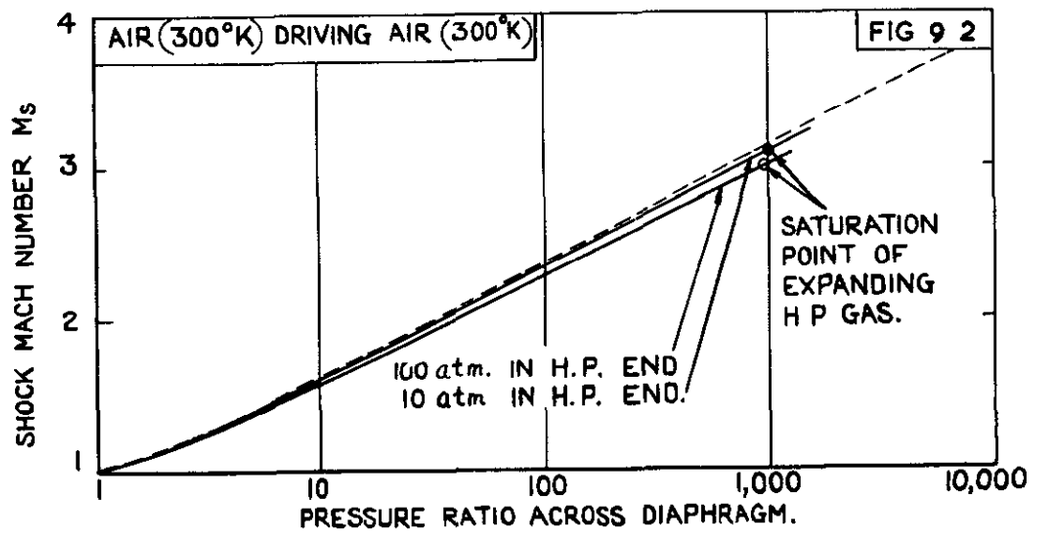

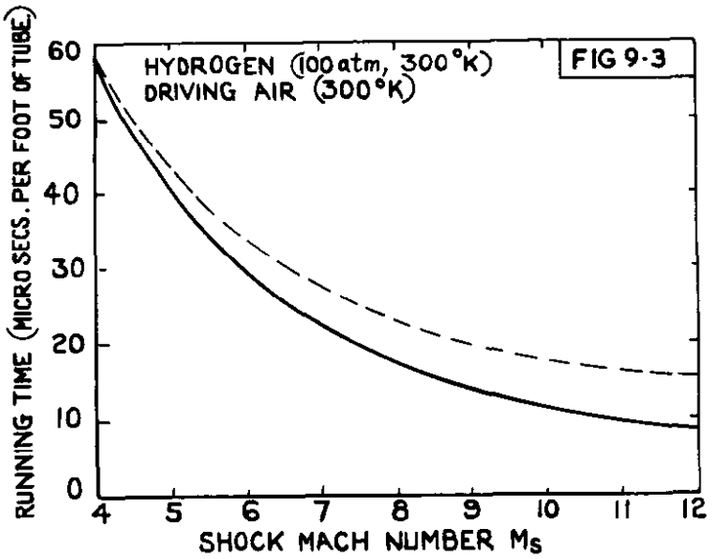

FIG. 9. SHOCK TUBE PERFORMANCE.

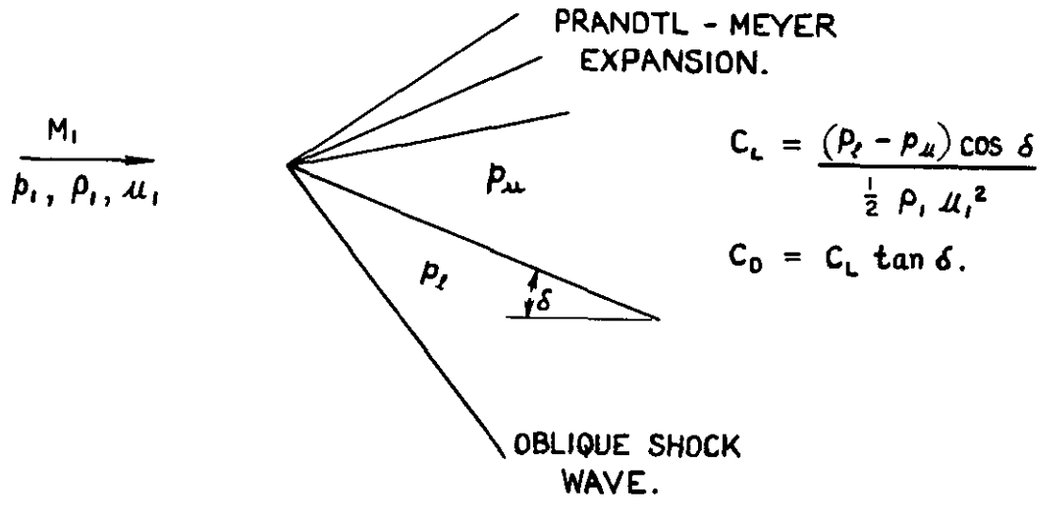

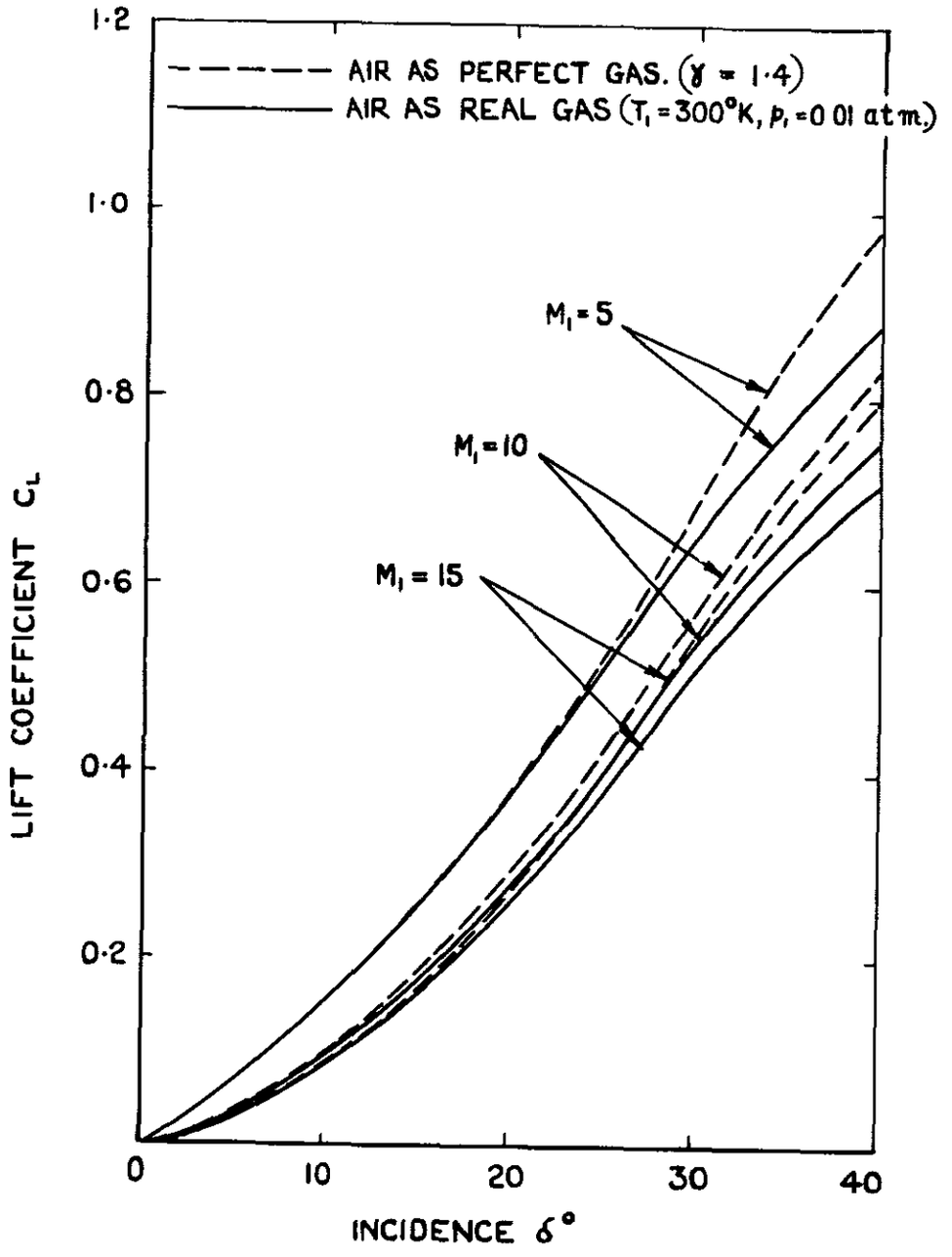

FIG.10. LIFT OF FLAT PLATE.

(NOTE:- "y" SCALE MAGNIFIED × 5.)

_ _ _ _ PERFECT GAS (γ = 1·4, INLET MACH NUMBER = 1·85)

———— REAL GAS (AIR, INLET MACH NUMBER = 2·5, TEMPERATURE = 5,000 °K, PRESSURE = 100 atm)

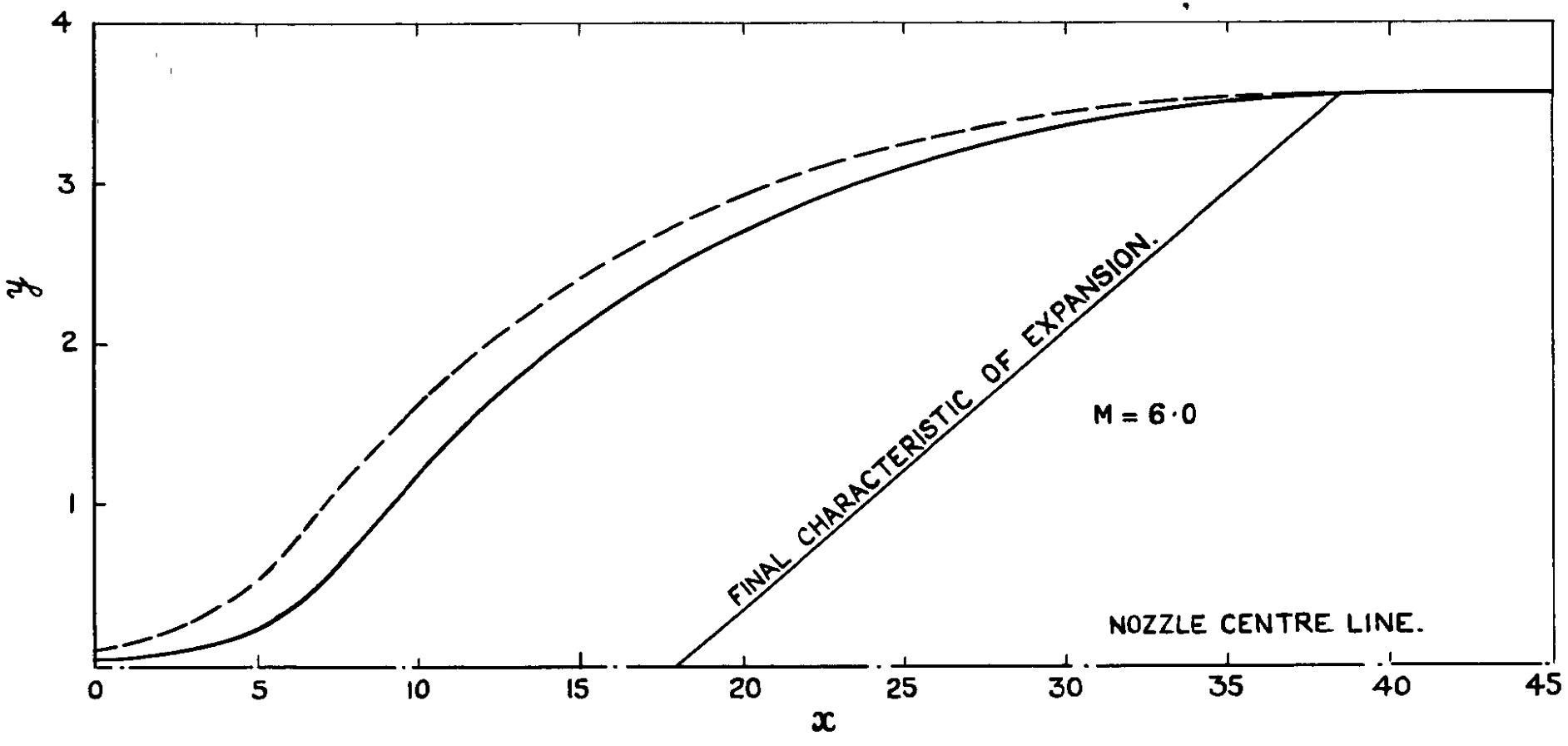

FIG.11. NOZZLE OF HYPERSONIC IMPULSE TUNNEL.

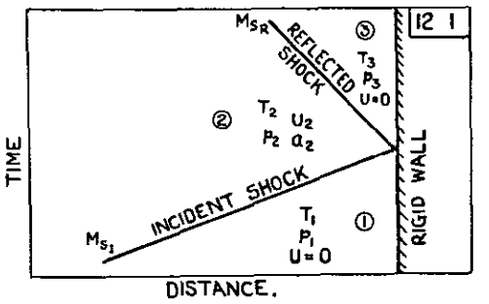

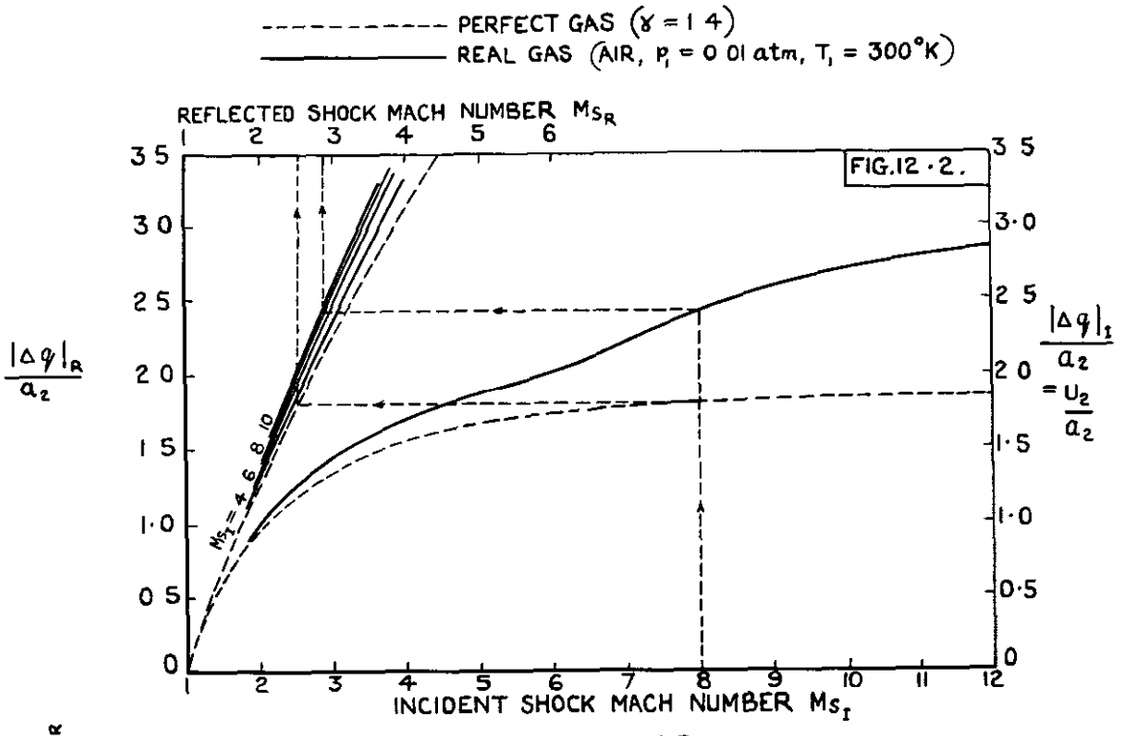

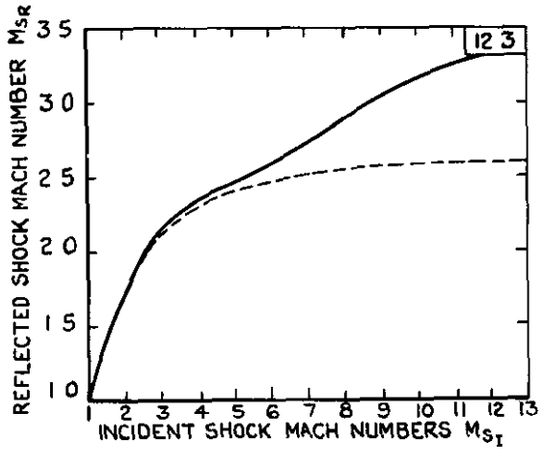

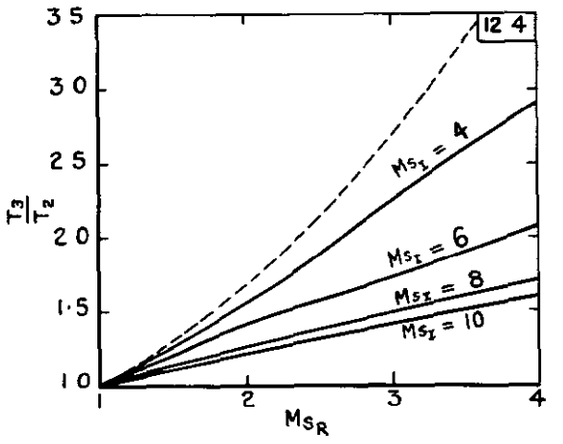

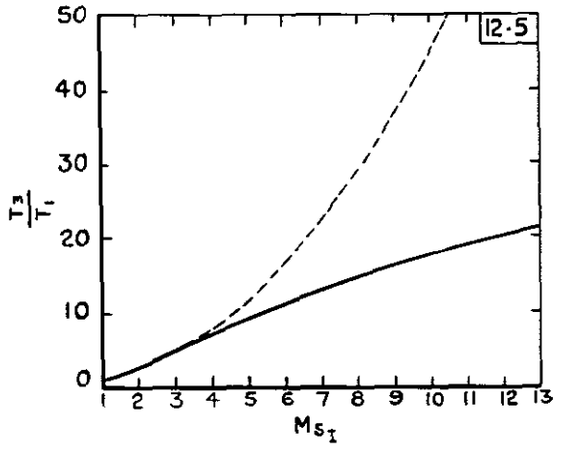

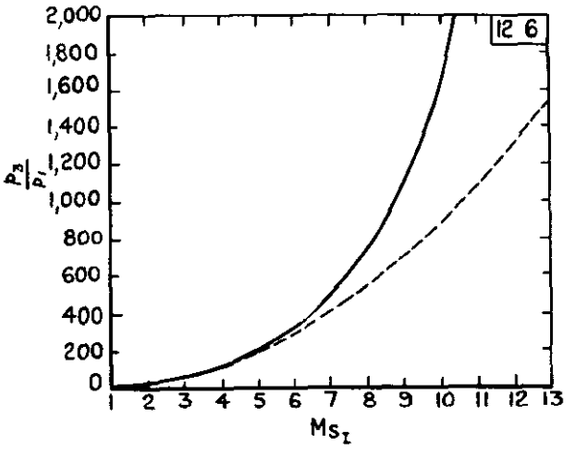

FIG.12. REFLECTION OF NORMAL SHOCK WAVE FROM RIGID WALL.

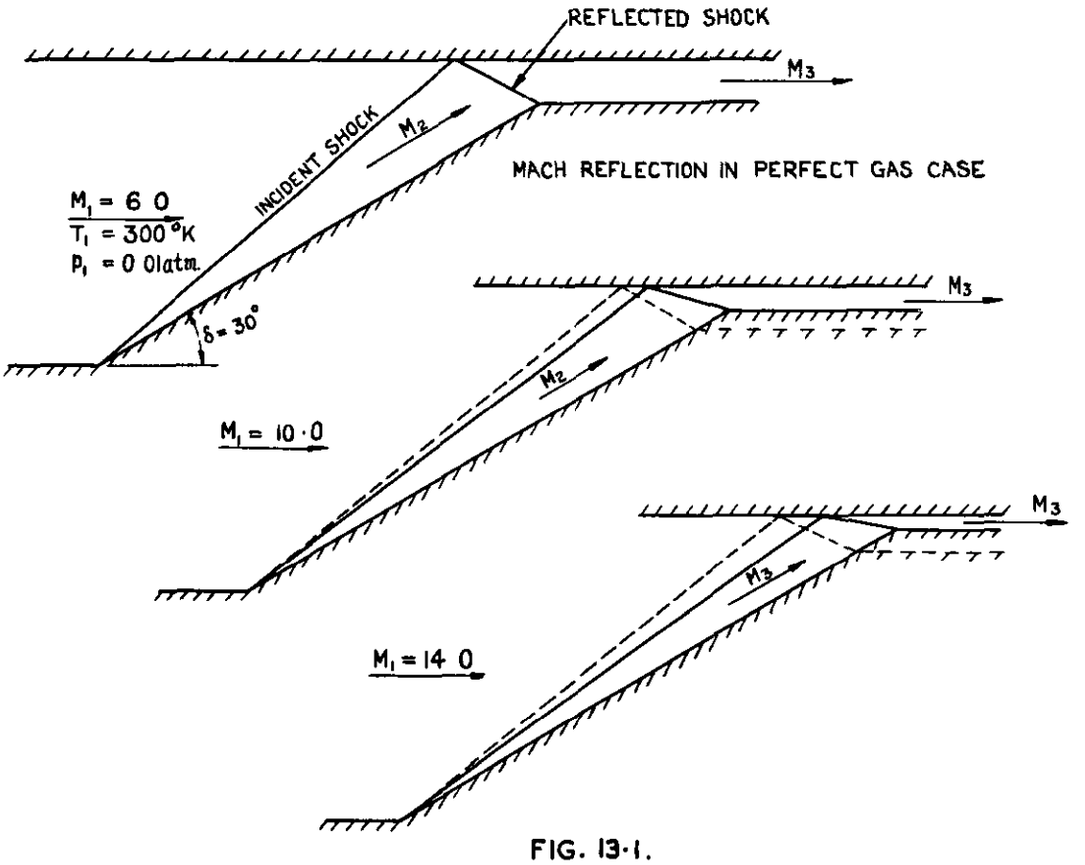

FIG. 13·1.

PERFECT GAS ($\gamma = 1{\cdot}4$)
REAL GAS (AIR, $T_1 = 300\,^{\circ}K$. $p_1 = 0\ 01\ atm$)

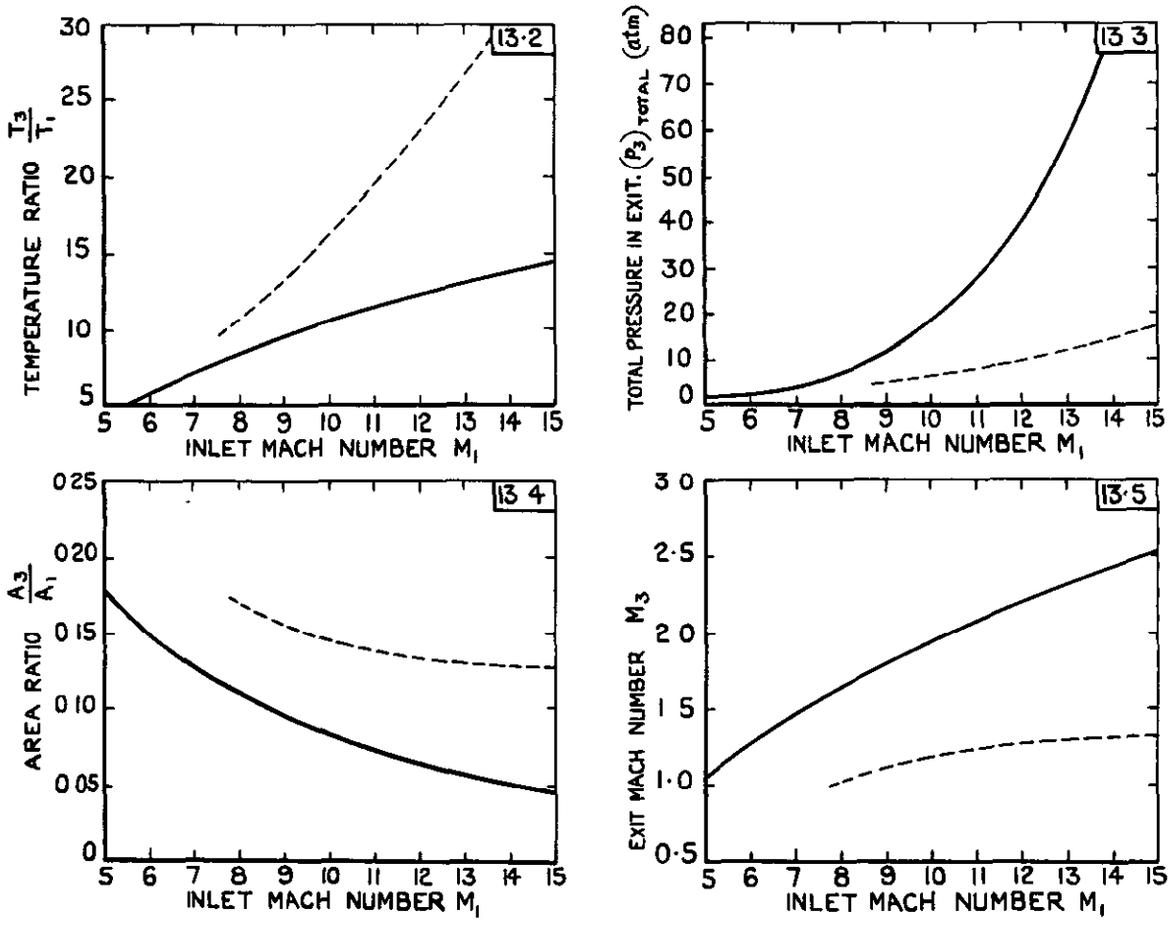

FIG.13. TWO — DIMENSIONAL SUPERSONIC INTAKE.
(OBLIQUE SHOCK COMPRESSION)

C.P. No. 397
(19,547)
A.R.C. Technical Report

Published by
HER MAJESTY'S STATIONERY OFFICE

To be purchased from
York House, Kingsway, London w.c.2
423 Oxford Street, London w.1
13A Castle Street, Edinburgh 2
109 St. Mary Street, Cardiff
39 King Street, Manchester 2
Tower Lane, Bristol 1
2 Edmund Street, Birmingham 3
80 Chichester Street, Belfast
or through any bookseller

PRINTED IN GREAT BRITAIN

S.O. Code No. 23-9010-97

C.P. No. 397